Universiteit Antwerpen

This item is the archived peer-reviewed author-version of:

Functional antagonism of voltage-gated K+ channel alpha-subunits in the developing brain ventricular system

Reference:
Shen Hongyuan, Bocksteins Elke, Kondrychyn Igor, Snyders Dirk, Korzh Vladimir.- Functional antagonism of voltage-gated K+ channel alpha-subunits in the developing brain ventricular system
Development - ISSN 0950-1991 - 143:22(2016), p. 4249-4260
Full text (Publisher's DOI): https://doi.org/10.1242/DEV.140467
To cite this reference: http://hdl.handle.net/10067/1526840151162165141

uantwerpen.be
Institutional repository IRUA

Development Advance Online Articles. First posted online on 11 October 2016 as 10.1242/dev.140467
Access the most recent version at http://dev.biologists.org/lookup/doi/10.1242/dev.140467

Functional antagonism of alpha-subunits of Kv channel in developing brain ventricular system

Hongyuan Shen[1], Elke Bocksteins[2], Igor Kondrychyn[1], Dirk Snyders[2], Vladimir Korzh[1,3,4].

[1]Institute of Molecular and Cell Biology, Singapore;

[2]Department for Biomedical Sciences, University of Antwerp, B-2610 Wilrijk, Belgium;

[3]Department of Biological Sciences, National University of Singapore, 117543, Singapore.

[4]Corresponding author: vlad@imcb.a-star.edu.sg;

Current address: International Institute of Molecular and Cell Biology, Warsaw, Poland.

Key words: Kcng4b, Kcnb1, neuroependyma extrusion, hydrocephalus, cell proliferation, tissue integrity.

Summary Statement: Development of the brain ventricular sytem in zebrafish depends upon activity of voltage-gated K channels that establishes a balance between cell proliferation and barrier properties in neuroepithelium that lines ventricles.

Development • Advance article

© 2016. Published by The Company of Biologists Ltd.

Summary

The brain ventricular system is essential for neurogenesis and brain homeostasis. Its neuroepithelial lining effects these functions, but the underlying molecular pathways remain to be understood. We found that the K channels expressed in neuroepithelial cells determine formation of the ventricular system. The phenotype of a novel zebrafish mutant characterized by denudation of neuroepithelial lining of the ventricular system and hydrocephalus is mechanistically linked to Kcng4b, the homologue of the "silent" voltage-gated K channel alpha-subunit Kv6.4. We demonstrated that Kcng4b modulates proliferation of cells lining the ventricular system and maintains their integrity. The gain of Kcng4b function reduces brain ventricles. Electrophysiological studies supported an idea that Kcng4b mediates its effects via an antagonistic interaction with Kcnb1, the homologue of the electrically active delayed rectifier K channel subunit Kv2.1. The mutation of *kcnb1* reduces the size of ventricular system and its gain of function causes hydrocephalus, i.e. opposite to the Kcng4b function. This demonstrates the dynamic interplay between K channel subunits in the neuroepithelium as a novel and critical regulator of ventricular development in the vertebrate brain.

Development • Advance article

Introduction

The brain ventricular system (BVS) is evolutionarily conserved in vertebrates: formed by a series of inter-connected cavities filled with cerebrospinal fluid (CSF) and surrounded by a neuroepithelium of ependymal cells, it plays an essential role in regulating neurogenesis, brain function, and homeostasis. Dysregulation of the BVS causes hydrocephalus (Zhang et al., 2006; Green et al., 2007; Tully and Dobyns, 2014). It has been linked to neurodegenerative diseases (Sakka et al., 2011). This led to interest in animal models of hydrocephalus recapitulating the disturbance of CSF circulation and showing changes in the neuroepithelium integrity (Chae et al., 2004; Chang et al., 2012; Jimenez et al., 2001). In the adult brain, CSF is produced mainly by the choroid plexuses (CP, Johanson, 2003). During human development brain ventricles inflate several weeks prior to CP formation (Bayer and Altman, 2008). Similarly in zebrafish the ventricles begin inflating at 19 hours post fertilization (hpf) (Lowery and Sive, 2005), i.e. prior to formation of CP at 48 hpf (Bill et al., 2008; Garcia-Lecea et al., 2008). Therefore, an early evolutionarily conserved CP-independent mechanism must exist producing embryonic CSF (eCSF) for ventricle inflation. Molecular analysis of the fundamental mechanisms of neurulation has shown their conservation across vertebrate species (Copp et al. , 2003; Harris and Juriloff, 2010; Korzh, 2014). The formation of the ventricular system begins with the fourth ventricle (hindbrain), followed by the third ventricle (forebrain), and the central canal of the spinal cord (Lowery and Sive, 2005; Garcia-Lecea et al., 2008; Kondrychyn et al., 2013).

Inflation of the BVS requires increased intraluminal pressure. It is thought that this is achieved by a combination of increased production of eCSF by neuroepithelial (ependymal) cells, which also function as neural stem cells (Desmond, 1985; Desmond and Levitan, 2002; Johansson et al., 1999; Lowery and Sive, 2005; Mirzadeh et al., 2008; Meletis et al., 2008; Hamilton et al., 2009; Guo et al., 2011), and/or restriction of neuroepithelial permeability

Development • Advance article

(Chang et al., 2012; Fossan et al., 1985; Lowery and Sive, 2009; Whish et al., 2015). While the mechanisms regulating the ventricular lining remain unclear, the expression of voltage-gated potassium (K_v) channels by ependymal cells might be essential due to their role in cell proliferation (Smith et al., 2008).

K_v channels are K^+ selective transmembrane proteins with the central pore surrounded by four individual alpha subunits that contain six transmembrane segments (S1–S6) and cytoplasmic NH2- and COOH- termini (Long et al., 2005). Several potassium currents, including both slow-inactivating delayed rectifier (I_K) and fast-inactivating A-type transient outward (I_A) currents, have been detected in neuronal stem cells (NSC) and neuronal progenitor cells (NPC) (Aprea and Calegari, 2012; Blackiston et al., 2009; Cai et al., 2004; Li et al., 2008; Liebau et al., 2006; Smith et al., 2008). *In vitro*-derived NSCs and mesenchymal stem cells (MSC) express $K_v1.3$, $K_v3.1$ and $K_v2.1$ subunits, implicating these in I_K current (Deng et al., 2007; Smith et al., 2008). However, the composition of K_v channels underlying I_K and I_A currents varies depending of the differentiation and/or proliferation state of the NSCs and NPCs. The relevance of these observations to development of the brain ventriculart system remains unclear.

Members of the K_v2 subfamily (i.e. $K_v2.1$ and $K_v2.2$ encoded by the *Kcnb1* and *Kcnb2* genes, respectively) play an important role in neuronal excitability (Vacher et al., 2008). They assemble into functional heterotetrameric channels with modulatory "silent" K_v (K_vS) subunits (Bocksteins and Snyders, 2012). The $K_v6.4$ is a typical K_vS subunit, which, upon assembly with $K_v2.1$ at the endoplasmic reticulum, forms a heterotetramer transported to the plasma membrane. Relative to $K_v2.1$ homotetramers $K_v6.4$ reduces the current density, shifts the voltage-dependence of inactivation approximately 40 mV into hyperpolarized potentials and slows the activation and deactivation kinetics (Ottschytsch et al., 2002; Bocksteins et al., 2009).

Development • Advance article

Here, we investigated the role of K^+ channels in development of the BVS. Using a *Tol2* transposon-mediated 'gene-breaking' insertional mutagenesis of zebrafish (Sivasubbu et al., 2006; Clark et al., 2011) we identified the *kcng4b* mutant due an over-inflated IVth ventricle. We demonstrated that Kcng4b, a zebrafish homologue of the "silent" $K_v6.4$ subunit, regulates proliferation of neuroepithelium lining the ventricular cavity and maintains its integrity critical for ventricles inflation by modulating the $K_v2.1$ activity, which opposes that of $K_v6.4$ during formation of the BVS. Taken together these results establish the Kcng4-Kcnb1 axis as a developmental regulator of the BVS in vertebrates.

Development • Advance article

Results

Insertional mutagenesis identifies *kcng4b* mutant

To determine novel molecular determinants of the BVS, we performed a forward genetic screen in zebrafish using *Tol2*-transposon-based insertional mutagenesis with a "gene-breaking transposon" (GBT) cassette (Sivasubbu et al., 2006) (Fig. S1). Once inserted into the intronic sequence by *Tol2*-transposition, it disrupts splicing, with nearly all tested fish lines displaying >95% reduction in native transcript abundance (Sivasubbu et al., 2007; Clark et al., 2011). Using this strategy we generated 61 zebrafish lines bearing germ-line inactivating integrations; one of these mapped to the second intron of *kcng4b* (Chr. 7, Zebrafish Information Network - http://zfin.org/ZDB-GENE-130530-634; Fig. 1, H) was characterized by appearance of cells in the third ventricle (24 hpf, N=525/525; 100%), hydrocephalus (48 hpf, N=411/525; 78%), cardiac oedema (Fig. 1, A-G), and a reduction of intersomitic vessels (not shown).

Apart from *kcng4b*, the zebrafish genome harbours *kcng4a* (Chr.18, ENSDARG00000062967, Ensembl Zv9). Comparison of Kcng4a and Kcng4b with K_v6.4 and K_v2.1 demonstrated an evolutionary conservation of functional domains characteristic of mammalian Shaker-related K_v subunits: proteins from both species possess six transmembrane segments (S1-S6), a pore loop containing the K^+ signature sequence GYG, several positively-charged residues on the S4 segment that function as voltage sensor, and a tetramerization domain T1 on the cytoplasmic N-terminus (Long et al., 2005; Fig. S2A). However, compared to mammalian K_v6.4, the two putative zebrafish Kcng4s have a longer C-terminus. The mutation causes the premature termination of *kcng4b* transcript at R249 resulting in a transcript similar to the short splice variant predicted for human *KCNG4* and zebrafish *kcng4a*. Based on sequence homology such transcript encodes a truncated

Development • Advance article

polypeptide Kcng4b* that contains a segment of Kcng4b with the N-terminus, S1 segment and partial S1-S2 linker (Fig. 1I and Fig. S2B). Kcng4b* is structurally similar to the truncated K_v1.1 and K_v1.5 that exert *in vitro* the relatively weak dominant-negative effect (Babila et al, 1994). Hence, the zebrafish mutant provides a unique opportunity to understand the developmental impact of such a truncation of a modulatory subunit of K channel.

Reverse Transcription-PCR (RT-PCR; Fig. 1J) on 30 hpf wild-type (*kcng4b*$^{+/+}$), heterozygous (*kcng4b*$^{+/-}$) and homozygous (*kcng4b*$^{-/-}$) embryos revealed a reduction of full-length *kcng4b* transcripts in *kcng4b*$^{+/-}$, and their absence in *kcng4b*$^{-/-}$ (Fig. 1J). Thus expression of native *kcng4b* was effectively ablated by GBT cassette insertion. To confirm that the mutant phenotype was due to *kcng4b* loss-of-function (LOF), we injected wild-type embryos with anti-sense morpholino oligonucleotides (MO) inhibiting splicing of *kcng4b* at the intron2-exon3 junction (Fig S3A, B) and observed the same phenotype (Fig. S3C). Hence, LOF of *kcng4b* caused by insertional mutagenesis or MO-mediated knockdown caused the same defects in the BVS.

kcng4b is expressed in the ventricular zone

To define the developmental expression profile of *kcng4b*, we used RT-PCR at timepoints preceding emergence of the mutant phenotype. *kcng4b* is expressed in a biphasic manner with the first transient expression phase at the end of epiboly (8-9 hpf) and the second phase starting at 21 hpf (Fig. 2A, A'). Full-length transcripts were not detected in the adult tissues examined (Fig. 2B) indicating that *kcng4b* functions only in development. Whereas the first phase of *kcng4b* expression (8-9 hpf) might be linked to formation of the Kuppfer vesicle, the second phase of *kcng4b* expression correlates with formation of the brain ventricular system at 18 - 22 hpf (Lowery and Sive, 2005). Whole mount *in situ* hybridization (WISH) using antisense RNA probes revealed expression of *kcng4b* in the ventricular zone and central canal

Development • Advance article

(24-48 hpf, Fig. 2C,E-H), extended yolk and otic vesicle (30 hpf, Fig. 2G,G''; 48 hpf, Fig. 2, H'), ciliary retina, lenses (48 hpf, Fig. 2H', inset), and intersegmental vessels (48 hpf, Fig. 2H''). The sense probe showed no staining (Fig. 2D).

To distinguish developmental roles of the two *kcng4s*, we cloned *kcng4a*. At 24-48 hpf *kcng4a* was expressed in the lens, similar to *kcng4b*, and in the cranial sensory ganglia and Rohon-Beard sensory cells of the spinal cord (Fig. 2, F). Therefore, with the exception of the developing eye, *kcng4a* and *kcng4b* exhibit distinct expression patterns: importantly, only *kcng4b* is expressed in the brain ventricular system. The mutant phenotype of *kcng4b*$^{-/-}$ correllates with expression of *kcng4b* (Fig. 2). The divergence of expression patterns of the two *kcng4s* supports a specific role of *kcng4b* in development of the BVS.

kcng4b is required for integrity of the ventricular zone

The primary *kcng4b*$^{-/-}$ phenotype is presence of cells in the forebrain ventricle. It prompted detailed evaluation of the ventricular zone of mutant embryos. ZO-1, αPKC and F-actin identify the apical surface of the neuroepithelium (Munson et al., 2008). A distribution of ZO-1 and αPKC at 24 hpf on confocal sections (Fig. 3A-H) as well as αPKC at 24 hpf (Fig. S4) and F-actin at 48 hpf (Fig. S4) on cryosections was examined by fluorescence microscopy. In wild-type embryos anti-ZO-1 and anti-αPKC immunolabeling revealed a smooth apical surface, while in *kcng4b* morphants it was distorted (Fig. 3E', G'; Fig. S4C,D). In the forebrain ventricle cells were found in the lumen (Fig. 3A'-H'; Fig. S4A,B). At 48 hpf the dorsal wall of the neural tube is very thin in mutants and lacks organized F-actin staining (Fig. S5A-D). Hence loss of function of *kcng4b* affects cell polarity in the ventricular zone.

Neuroepithelial cells lining the brain ventricles retain eCSF within the lumen (Lowery and Sive, 2009), and the integrity of this barrier could be measured using a dye retention assay (Chang et al., 2012) (Fig. 3I-P). Following injection of 70kDa FITC-Dextran into brain

Development • Advance article

ventricles at 24 hpf, the distance that dye front spread from the forebrain was analysed (Fig. 3K-L; blue scale bar). It was found that within 60' the dye spread in mutants much more than that in controls (Fig. 3M, N). This indicated that the integrity of mutant neuroepithelium was compromised. We investigated this further by detailed confocal imaging of the neuroepithelium of *kcng4b* morphant embryos in *Tg(h2b:EGFP)* background (Fig. 3R-Z). Here Dextran-TexasRed penetrated into the mutant forebrain neuroepithelium 30' after its injection into the IVth ventricle (Fig. 3V,V'), but not in midbrain and hindbrain neuroepithelium (Fig. 3Z, Z'; n = 6). Therefore, disruption of neuroepithelium integrity mainly happens at the forebrain region in *kcng4b*-deficient embryos.

kcng4b modulates brain inflation

The secondary effect of *kcng4b* LOF is hydrocephalus. We quantified this phenomenon by measururing a volume of the BVS in 48 hpf controls and mutants. 3D-reconstruction of confocal Z-scans showed that in the mutant this system enlarged almost 3X (Fig. 4A-C). To show an effect of Kcng4b gain-of-function (GOF) on ventricular development *kcng4b* mRNA was injected into 1-2 cell stage wild-type embryos and at 21-24 hpf they were soaked in FITC-BODIPY (Lowery and Sive, 2005). The hindbrain ventricle forms at 21 hpf and expands at 24 hpf, when the midbrain lumen (optocoele) forms. Hence, initial brain inflation and subsequent lumen expansion were monitored at 21-24 hpf (Fig. 4F-J). According to analysis of the body axis, somite number and formation of the midbrain-hindbrain boundary (MHB), the Kcng4b GOF embryos developed relatively normal (Fig. 4D,E) except that at 21 hpf the hindbrain ventricle did not form (Fig. 4G) and at 24 hpf it did not form and/or expand and the optocoele failed to form (Fig. 4I,J). Thus, Kcng4b GOF embryos displayed a phenotype opposite to that of Kcng4b LOF (Fig. 4A-C).

Development • Advance article

Next we asked whether the function of Kcng4b is conserved in evolution. We injected wild-type embryos with a construct encoding C-terminal EGFP-tagged human K_v6.4. This affected inflation of brain ventricles similar to that of Kcng4b GOF (Fig. S6) suggesting that human K_v6.4 may regulate formation of ventricles.

kcng4b inhibits cell proliferation

During neurogenesis in mammals and zebrafish, the nuclei of dividing neuroepithelial cells prior to mitosis undergo interkinetic nuclear migration (INM) towards the apical surface, where round-shaped cells appear (Merkle and Alvarez-Buylla, 2006; Gutzman and Sive, 2010; Leung et al., 2011). Such cells were often found close to the midbrain lumen in 24 hpf wild-type embryos (Fig. 4H''; arrowhead; n = 22 per confocal section). In contrast, upon *kcng4b* GOF proliferating cells were less numerous (n = 6 per confocal section; Fig. 4I''). These results suggested that Kcng4b modulates proliferation of neuroepithelial cells of the BVS.

To extend this analysis an impact of Kcng4b on cell proliferation was analyzed by quantifying the phospho-histone-3 (PH3)-positive (M-phase) cells. The majority of the PH3-positive cells were near the lumen (Fig. 5A,D,G). The number of the PH3-positive cells and the proliferative index (the number of PH3-positive cells per one thousand neuroepithelial cells) in 24 hpf *kcng4b* GOF embryos was significantly lower than that in controls (Fig. 5B, C). In contrast, analysis of *kcng4b*$^{-/-}$ mutants demonstrated significant increase in PH3-positive cells (Fig. 5D,I). Whereas during development cell proliferation decreases, in *kcng4b*$^{-/-}$ mutants this trend is less obvious as reflected by the difference in proliferative index between *kcng4b*$^{-/-}$ mutants and wild-type controls, which increased from 2-fold (24 hpf) to almost 3-fold (48 hpf). Taken together, these results demonstrated that Kcng4b modulates cell proliferation.

Development • Advance article

Kcng4b modulates K_v2.1 activity

To analyze Kcng4b function further we expressed full-length Kcng4b in human cell lines for electrophysiological characterization. Similar to human K_v6.4 (Ottschytsch et al., 2002), zebrafish Kcng4b alone did not form electrically-active channels at the plasma membrane (data not shown). However, upon co-expression with K_v2.1, the zebrafish Kcng4b probably assembled into functional K_v2.1/Kcng4b heterotetramers since this caused modulation of biophysical properties compared to K_v2.1 homotetramers (Fig. 6). Typical current recordings of K_v2.1/Kcng4b heterotetramers are shown in Figure 6A. K_v2.1/Kcng4b channels display a voltage-dependence of activation and of inactivation that is characterized by $V_{1/2}$ = -22.1 ± 1.5 mV (n = 9) and $V_{1/2}$ = -52.8 ± 2.5 mV (n = 5), respectively (Fig. 6B). Furthermore K_v2.1/Kcng4b heterotetramers displayed two components in their timecourse of activation (Fig. 6C). In addition, Kcng4b also reduced the K_v2.1 current density; the K_v2.1 + Kcng4b co-expression displayed a current density of 1115 ± 214 pA/pF (n = 9, Fig. 6D) at 40 mV while the same amount of transfected K_v2.1 cDNA (co-expressed with CFP to exclude possible effects of DNA dilution and/or an overload of the translational machinery) resulted in current too large to clamp at 40 mV without any voltage errors (not shown). The biophysical properties of these Kv2.1/Kcng4b heterotetramers are very similar to those of Kv2.1/Kv6.4 channels indicating that zebrafish Kcng4b modifies the biophysical properties of Kv2.1 in a similar way as human Kv6.4; human Kv6.4 shifts the Kv2.1 voltage dependence of inactivation almost 40 mV to hyperpolarized potentials, introduces a second time constant in the Kv2.1 activation time course and reduces the Kv2.1 current density (David et al., 2015). In contrast to full-length Kcng4b, co-expression of Kv2.1 and Kcng4b* did not result in the typical Kv6.4-induced modulations of the Kv2.1 activation, inactivation

Development • Advance article

and deactivation properties (Fig. 6). Typical current recordings obtained after co-expression of Kv2.1 with Kcng4b*, are shown in Figure 6A. Co-expression of Kv2.1 with Kcng4b* resulted in a voltage dependence of activation and of inactivation that is characterized by $V_{1/2}$ = 6.7 ± 1.6 mV (n = 5) and $V_{1/2}$ = -15.0 ± 3.1 mV (n = 5), respectively, which are both significantly different ($p < 0.05$) compared to that of Kv2.1/Kcng4b heterotetramers (Fig. 6B). Furthermore, co-expression of Kv2.1 with Kcng4b* yielded an activation time course characterized by only one component and the time course of deactivation was accelerated compared to that of Kv2.1/Kcng4b heterotetramers (Fig. 6C). The biophysical properties obtained upon co-expression of Kv2.1 with Kcng4b* are very similar to those of Kv2.1 homotetramers (David et al., 2015) suggesting that Kcng4b* did not tetramerize with Kv2.1. However, co-expression of Kv2.1 and Kcng4b* reduced the current density to an even greater extent than co-expression of native Kcng4b; Kcng4b* reduced the current density to 606 ± 184 pA/pF (n = 9, Fig. 6D) at 40 mV, where the open probability of both Kv2.1/Kcng4b and Kv2.1/Kcng4b* channels is 1 excluding the possibility that the differences in current density reflects the difference in open probability. This suggested that Kcng4b* does interact with K_v2.1 and exerts a dominant-negative effect, as has been demonstrated for the dominant-negative mutants of K_v1.5 and K_v2.1 (Babila et al., 1994; Xu et al., 1999). Taken together the developmental and electrophysiological analysis of the *kcng4b* mutant demonstrated that the mutant phenotype resulting from the LOF of Kcng4b function has been further compounded by the dominant-negative effect of Kcng4b*.

Functional antagonism of *kcnb1* and *kcng4b*.

These results supported an idea that Kcng4b modulates activity of K_v2.1, which in zebrafish is encoded by a single *kcnb1* gene (Chr. 6, ENSDARG00000060095, Ensembl Zv9). The WISH demonstrated that *kcnb1* is expressed in the BVS, central canal and otic vesicles at 24-

Development • Advance article

30 hpf (Fig. 7A,B), similar to *kcng4b* (Fig. 2C-E). At 48 hpf the expression domains of these genes include the BVS, eyes and ears (Fig. S7). To explore a developmental role of *kcnb1*, we performed GOF analysis by injecting *kcnb1* mRNA into zebrafish embryos, which in a fraction of 24 hpf embryos resulted in a clump of cells in the forebrain ventricle (Fig. 7C,D; N=218/325; 67%) and at 48 hpf caused hydrocephalus (Fig. 7E,F; N=42/218; 19%). Thus the phenotype of Kcnb1 GOF phenotypically mimicks that of the *kcng4b* mutant (Fig. 1A-D). This again pointed at the functional antagonism of members of the Kcng4b/Kcnb1 axis during formation of the BVS.

To further validate the functional role of Kcnb1 during ventricle formation, we generated the *kcnb1* mutant by the CRISPR-Cas9 mutagenesis (Hwang et al. 2013). The single-guide RNA (sgRNA) targeted zebrafish *kcnb1* downstream of the sequence encoding the NAB domain (Fig. 7E). Following *Cas* mRNA injection T7E1 assay documented an induction of molecular lesions at the targeted site. Adult F_0 animals were screened for stable mutations inherited by F_1 progeny. We isolated three different *kcnb1* indel (insertion/deletion) mutants, including two with premature stop codons (Fig. 7E, #1, #2). *kcnb1*$^{-/-}$ displayed two distinct phenotypes: the early one - delayed epiboly and gastrulation failure (Fig. S8B). Some *kcnb*1 mutants completed gastrulation and displayed the late phenotype - reduced brain ventricles (Fig. 7F, G). As shown by FITC-Dextran labeling, 24 hpf *kcnb1*$^{-/-}$ failed to inflate the midbrain and partially inflated the hindbrain.

These results further supported the functional antagonism of members of the Kcng4b/Kcnb1 axis during formation of the BVS. Embryos with epiboly and brain ventricle phenotype constitute about 9-14% of the progeny of *kcnb1*$^{-/+}$ parents of both alleles (#1, #2) (Fig. S8B) illustrating incomplete mutation penetrance. Taken together, these results demonstrated a novel function of the voltage-gated K channels in regulating development of the BVS, which involves modulation of Kcnb1 (K_v2.1) activity by Kcng4b (K_v6.4).

Development • Advance article

Discussion

$K_v2.1/K_v6.4$ axis regulates formation of the brain ventricular system.

Several electrically-active subunits of voltage-gated potassium (K_v) channel contribute to the neuronal delayed rectifier K^+ current (I_{DR}) regulating cell proliferation and excitability in the CNS (Wonderlin and Strobl, 1996; Pardo, 2004; Vacher et al., 2008). *Kcnb1*-encoded $K_v2.1$ contributes into K^+ channels that form a major I_{DR} component in hippocampal and DRG neurons (Murakoshi and Trimmer, 1999; Du et al., 2000; Bocksteins et al., 2009). Moreover, it has been suggested that the electrically-silent K_v (K_vS) subunits modulate the K_v2-mediated current; K_v2/K_vS heterotetrameric channels carry approximately 30% of the K_v2-containing I_{DR} current in DRG neurons (Bocksteins et al., 2009).

Our study demonstrated that the *kcng4b* and *kcnb1* encoding homologues of the mammalian $K_v6.4$ and $K_v2.1$, respectively, display expression in the ventricular neuroepithelium (Fig. 2, 7). *Kcng4* expression was also detected in the ventricular neuroepithelium of developing mice (http://developingmouse.brain-map.org/gene/show/42576) (Lein et al., 2007). Coincidentally, the *kcng4b* mutation causes formation of Kcng4b*, similar to polypeptides with a dominant-negative effect on K_v activity *in vitro* (Babila et al, 1994). The native short transcripts of the human *KCNG4* and zebrafish *kcng4a* might be involved in development of sensory neurons, etc. Hence several elements of expression of Kcng4 seems are conserved in evolution suggesting a conservation of its developmental roles in vertebrates.

Kcng4b regulates neuroepithelial cell proliferation

The interplay between activities of different K_v channels determines the proliferative state of various cells/tissues (Wonderlin and Strobl, 1996; Pardo, 2004; Deng et al., 2007). While selective blockage of $K_v1.3$ and $K_v3.1$ channels increases the proliferation rate of

Development • Advance article

mesencephalic NPCs, pharmacological blockage of K_v2.1 inhibits cell proliferation in rat MSCs (Pardo, 2004). The combined electrophysiology and genetic analysis revealed the likely interaction between Kcng4b and Kcnb1; however, Kcng4b may interact with other electrically-active subunits of K_v channels. Recently, we demonstrated that the N-terminus of K_v6.4 interacts with that of K_v3.1 without the formation of functional heterotetrameric channels (Bocksteins et al., 2014). This suggests that Kcng4b* may interact with K_v3.1 and that Kcng4 LOF could increase cell proliferation by reducing the K_v3.1 current via the non-functional K_v3/Kcng4* "channels". Further developmental analysis of relevant K_v channels will be required in future.

An increase in the surface area of the neuroepithelial layer further increases the proliferation of neuroepithelial cells, and where the ventricular lining become overcrowded, cell extrude to preserve barrier function (Rosenblatt et al., 2001; Gu and Roseblatt, 2012). This may explain the appearance of cells in the third ventricle (Fig. 1C'-D'; 3A-D; Fig. 7D). Conversely, overexpression of Kcng4b would reduce K_v channel activity at the plasma membrane, which could alter the membrane potential of neuroepithelial cells towards depolarization and decrease cell proliferation (Fig. 5A-C) in parallel with deficient inflation of brain ventricles (Fig. 4G, I). Therefore, our data support a role of voltage-gated K channels in the modulation of neuroepithelial cell proliferation coupled to ventricle inflation.

Kcng4b maintains integrity of the neuroepithelium

Formation of brain ventricles requires both production of eCSF and its retention. The latter function may be accomplished by the neuroepithelial barrier lining the ventricles (Chang et al., 2012; Fossan et al., 1985; Lowery and Sive, 2009; Whish et al., 2015). In the *kcng4b* mutant, this layer is compromised (Fig. 3A-D; Fig. S4, 5) failing to maintain an expansion of ventricular system within physiological limits and retain FITC-dextran (Fig. 3E-N)

Development • Advance article

coincidental with the abnormal ventricular system induced by changes in Kcnb1 activity (Fig. 7). This further supports the idea that the voltage-gated K channels regulate formation of the polarized and continuous neuroepithelial layer, which acts as a barrier to restrict a flow of eCSF. This hypothesis has been presented in more details in Fig. 8, although the exact molecular mechanism probably remain elusive until the transcriptome analyses of *kcng4b* mutant is performed.

Judging by an increased cell proliferation and extrusion of cells the integrity of neuroepithelial layer is compromised very early at least a day before hydrocephalus. Why cell extrusion happens in the third ventricle and not in the fourth one? It could be due to a thin roof of the hindbrain ventricle, which could better accommodate superfluous cells comparing to the forebrain ventricle surrounded by thick walls of the neural tube. These inherent differences in ventricles mechanics manifest themselves by much greater degree of hydrocephalic expansion in the hindbrain (Fig. 1F, G). The cell extrusion is much earlier and more common phenomenon comparing to hydrocephalus. This suggests that a defect of integrity of neuroepithelium probably is a primary defect. This is reminiscent of other mutants: Chang et al. (2012) described discontinuous and non-polarized cell layer lining the ventricles in NaKATPase (*atp1a1*)-deficient zebrafish embryos. The delamination (extrusion) of ventricular cells (as a primary defect) and hydrocephalus (as a secondary one) has been also described in *Napa* mutant (*hyh*) mice. The gene *Napa* encodes soluble N-ethylmaleimide sensitive factor (NSF) attachment protein alpha (αSnap), involved in SNAP receptor (SNARE)-mediated vesicle fusion in many cellular contexts (Chae et al., 2004). Similar to **α**-Snap $K_v2.1$ also plays a role in membrane vesicle trafficking and SNARE–mediated membrane fusion in both neurosecretory cells and sensory neurons (Feinshreiber et al., 2009, 2010) and is required for transport of $K_v6.4$ to the plasma membrane (Ottschytsch et al.,

Development • Advance article

2002). This functional connection might underlie the phenotypic similarity of the *hyh* and *kcng4b* mutants.

In summary, the insertional mutagenesis screen in zebrafish led to identification of a *kcng4b* mutant that develops cell extrusion in the BVS followed by hydrocephalus indicating a novel function of K^+ I_{DR} channels in regulating brain ventricle development. This further led to identification of the functional interplay between $K_v2.1$ and $K_v6.4$ subunits during brain morphogenesis and suggested that Kcng4b could be a novel risk factor of integrity of ependyma and hydrocephalus. By extension, other negative regulators of $K_v2.1$ channel activity represent a reserve pool of factors that could similarly contribute to hydrocephalus. In contrast, deficiency of $K_v2.1$ has been linked with epileptic encephalopathy (Torkamany et al., 2014). It is rather remarkable that the two proteins involved in the same developmental mechanism underlying formation of the BVS, could be linked to two different hereditary diseases. The intrinsic functional interplay of the "silent" K^+ channel subunit Kcng4b and the electrically active K^+ channel subunit Kcnb1 during formation of the BVS highlights the dysregulation of K_v channels as the shared origin of these diseases and warrants further investigation of this complex problem.

Development • Advance article

Materials and Methods

Animals

Wild-type zebrafish (AB, ZIRC) were maintained as described (Westerfield, 1995). All animal experiments were carried according to the regulations of Institutional Animal Care and Use Committee (Biological Resource Center of Biopolis, license no. 120787), which approved this study. Developmental stages are in hours post fertilization (hpf) at 28.5°C (Kimmel et al. 1995).

Tol2-mediated insertional and CRISPR/Cas mutagenesis

The GBT cassette and *Tol2* transposase mRNA were injected at one-cell stage (Sivasubbu et al., 2006). 697/4347 embryos showed mosaic GFP expression by 24 hpf. 350 adults were mated to wildtype fish, screened for stable F1 transgenics, and 61 founders with germ-line integrations identified. In founders of F1 subfamilies the germline transmission was 5-62%. Two fish from subfamily were randomly chosen for mapping GBT integration sites using the TAIL-PCR method (Liu and Whittier, 1995; Parinov et al., 2004) . Fish with multiple insertions were out-crossed to a single insertion state.

pDR274 and pMLM3613 (Addgene, USA) were used to generate the gRNA that targets the 'GGAGCTGGACTACTGGGGAG' sequence in *kcnb1* exon1 and Cas9 mRNA, respectively, and generate *kcnb1* mutant (Hwang et al., 2013).

Kcnb1-Kcng4 constructs and morpholinos

cDNA sequences of *kcng4a* and *kcng4b* were obtained using Expand Long reverse transcriptase kit (Roche Diagnostics) and RNA isolated as a template from pooled 24 hpf embryos using the RNeasy kit (Qiagen). The full length *kcng4b* was cloned into the pTNT vector (Promega) using the primers: [A] 5'-CCG CTCGAG GCCACC ATGCCCATCATCAGCAATG-3' and [B] 5'-TGC TCTAGA

Development • Advance article

TCAGATATCTTTGCAACATGC-3' with XhoI/Xba resctriction sites (underlined). The same primer pair (A and B) was used for RT-PCR detection of *kcng4b* transcripts. Plasmid pSP64-K_v6.4-EGFP contains the full-length C-terminal EGFP tagged human *KCNG4* (Ottschytsch et al., 2005). Full length *kcnb1* was cloned into pCS2+ vector using primers: 5' - CGC GGATCC GCCACC ATGGAGAAACCCTCGGCA' and CCG CTCGAG TCA AAG GCC CTT ATC AAA AG with BamHI/XhoI restriction sites (underlined). mRNA for microinjection was *in vitro*-transcribed using as templates the plasmids linearized at the 3'-end. 5'-capped RNA was synthesized using the mMessage T7/SP6 kit (Ambion). Transient knockdown of *kcng4b* was performed using a splice site-blocking MO (5'-TGCATTCGCCCTGTAAAAGAACAAA-3') targeting *kcng4b* intron 2-exon 3 (I2E3) junctions. Standard MO with the antisense sequence 5'-CCTCTTACCTCAGTTACAATTTATA-3' was used as a negative control. Morpholinos were designed by and purchased from GeneTools.

Whole mount *in situ* hybridization (WISH) and immunohistochemistry

WISH, immunohistochemistry and cryosections were performed following established protocols (Korzh et al., 1998; Kondrychyn et al., 2013). Anti-phosphohistone H3 (mouse, #06-570, Millipore), -αPKC (rabbit C20, sc-216, Santa Cruz), -ZO-1 (mouse, #33-9100, Invitrogen) primary antibodies were used for immunohistochemistry (1:200 in PBS). Secondary antibodies were AlexaFluor-488- or AlexaFluor-555-conjugated (Invitrogen) (1:500 in PBS) and AlexaFluor-555-conjugated Phalloidin and DAPI (1:500 in PBS). To quantify cell proliferation the PH3-labeled cells in each z-series were counted, averaged and, measured using ImageJ software. The approximate area occupied by each cell, total cell number and the percentage of labeled cells in each region were calculated.

BODIPY-FITC labelling of brain ventricles

FITC-conjugated Bodipy ceramide (Invitrogen) was dissolved in DMSO (5 mmol/l).

Development • Advance article

Embryos were soaked in 50 nmol/l Bodipy ceramide in egg water overnight in the dark at 28.5°C, washed, dechorionated and placed in 1% agarose wells (Lowery and Sive, 2005). Imaging was performed using the Zeiss LSM700 laser-scanning microscope (Zeiss). Images were processed by ImageJ software (NIH).

Dye retention assay

For dye retention assays (Chang et al. (2012) 70 kDa FITC-dextran (2.5 ng/ml in water) was injected into the brain ventricles at 22 hpf and imaged at 15 min intervals for 60 min. Neuroepithelial permeability was quantified using ImageJ to measure the distance of the dye front from respective forebrain ventricle hinge-points at a 20º angle relative to the embryonic midline. The net distance of the dye front diffusion was calculated by subtracting the distance at t=0 from other time points. Statistical analysis was performed and data plotted with Prism4 software (GraphPad).

Electrophysiology

Electrophysiological characterization of Kcng4b and Kcng4b* was performed using the whole-cell patch clamp. Human embryonic kidney (HEK293) cells obtained from the ATCC are yearly tested for contamination. The new vial (originating from the original culture) was thawed and cultured in enriched modified Eagle's medium supplemented with 10% fetal bovine serum, 1% non-essential amino acids and 1% penicillin-streptomycin (Invitrogen, San Diego, CA, USA) at 37°C and 5% CO_2. HEK293 cells were transiently co-transfected with $K_v2.1$ and Kcng4b or Kcng4b* cDNA using Lipofectamine2000 according the manufacturer's instructions. GFP was co-transfected as a transfection marker. Current recordings were obtained 24 hours post transfection using an Axopatch-200B amplifier (Axon Instruments) and were low-pass filtered and sampled at 1–10 kHz with a Digidata 1440 data acquisition system (Axon Instruments). The pClamp10 software (Axon Instruments) was used to command voltages and store data. Patch pipettes (with 1.5-2.5 MΩ

Development • Advance article

resistance) were pulled with a P2000 laser puller (Sutter Instruments) from borosilicate glass (World Precision Instruments). After heat polishing, patch pipettes were filled with an intracellular solution (ICS) containing 110 mM KCl, 5 mM K_4BAPTA, 5 mM K_2ATP, 1 mM $MgCl_2$ and 10 mM HEPES. Cells were continuously perfused with an extracellular solution (ECS) containing 145 mM NaCl, 4 mM KCl, 1.8 mM $CaCl_2$, 1 mM $MgCl_2$, 10 mM HEPES and 10 mM glucose. The pH of the ICS and ECS were adjusted to 7.2 and 7.35 with KOH and NaOH, respectively. Current recordings with voltage errors exceeding 5 mV after series resistance compensation were excluded from analysis. The voltage-dependence of activation and of inactivation was fitted with the Boltzmann equation $y = 1/\{1+\exp[-(V-V_{1/2})/k]\}$ with V the voltage applied, V1/2 the voltage at which 50% of the channels are activated or inactivated and k the slope factor. Activation and deactivation kinetics were fitted with a single or double exponential function.

Author Contributions:

HS – designed, performed and analyzed zebrafish experiments and wrote the manuscript;

IK –WISH;

EB – designed and performed electrophysiology experiments and wrote the manuscript;

DS – designed electrophysiology experiments, edited and approved the manuscript;

VK - designed zebrafish experiments, wrote and approved the manuscript.

Acknowledgements:

Authors declare no conflict of interests. They are thankful to Sridhar Sivasubbu and Stephen Ekker for the pX vector, Mr. Melvin Sin, Ms. Yi-chuan Chen and Ms Shelvi Ganda for

Development • Advance article

collecting data, the personnel of the IMCB Fish Facility for maintenance of zebrafish, Dr. Lucy Robinson of Insight Editing London for editing the manuscript and three anonymous reviwers for constructive comments. E.B. was supported by a postdoctoral fellowship from the Research Foundation – Flanders (FWO). HS was supported by the SERI-IMCB Program in Retinal Angiogenic Disease (SIPRAD) funded by the Agency for Science, Technology and Research of Singapore and VK lab at the IMCB by the institutional grant from the same agency.

References:

Aprea, J., Calegari, F. (2012) Bioelectric state and cell cycle control of mammalian neural stem cells. *Stem Cells Int.* **2012**, 816049.

Babila, T., Moscucci, A., Wang, H., Weaver, F.E., Koren, G. (1994) Assembly of mammalian voltage-gated potassium channels: evidence for an important role of the first transmembrane segment. *Neuron* **12**, 615-26.

Bayer, S.A., and Altman, J. (2008) The human brain during the early first trimester. Atlas of human central nervous system development, Boca Raton, FL; London, CRC.

Bill, B.R., Balciunas, D., McCarra, J.A., Young, E.D., Xiong, T., Spahn, A.M., Garcia-Lecea, M., Korzh, V., Ekker, S.C., Schimmenti, L.A. (2008) Development and Notch signaling requirements of the zebrafish choroid plexus. *PloS One* **3**, e3114.

Bill, B., and Korzh, V. (2014). Choroid plexus in developmental and evolutionary perspective. *Front Neurosci.* **8**, 363.

Bocksteins, E., Labro, A.J., Mayeur, E., Bruyns, T., Timmermans, J.P., Adriaensen, D., Snyders, D.J. (2009a). Conserved negative charges in the N-terminal tetramerization domain mediate efficient assembly of Kv2.1 and Kv2.1/Kv6.4 channels. *J. Biol. Chem.* **284**, 31625-31634.

Development • Advance article

Bocksteins, E., Raes, A.L., Van de Vijver, G., Bruyns, T., Van Bogaert, P.P., Snyders, D.J. (2009b). Kv2.1 and silent Kv subunits underlie the delayed rectifier K+ current in cultured small mouse DRG neurons. *Am. J Phys Cell Phys* **296**, C1271-1278.

Bocksteins, E., and Snyders, D.J. (2012). Electrically silent Kv subunits: their molecular and functional characteristics. *Physiology* **27**, 73-84.

Bocksteins, E., Mayeur, E., Van Tilborg, A., Regnier, G., Timmermans, J.P., Snyders, D.J. (2014). The subfamily-specific interaction between Kv2.1 and Kv6.4 subunits is determined by interactions between the N- and C-termini. *PLoS One* **9**, e98960.

Cai, J., Cheng, A., Luo, Y., Lu, C., Mattson, M.P., Rao, M.S., Furukawa, K. (2004) Membrane properties of rat embryonic multipotent neural stem cells. *J. Neurochem.* **88**, 212-26.

Chae, T.H., Kim, S., Marz, K.E., Hanson, P.I., Walsh, C.A. (2004) The hyh mutation uncovers roles for alpha Snap in apical protein localization and control of neural cell fate. *Nat. Genet.* **36**, 264-70.

Chang, J.T., Lowery, L.A., Sive, H. (2012). Multiple roles for the Na,K-ATPase subunits, Atp1a1 and Fxyd1, during brain ventricle development. *Dev. Biol.* **368**, 312-322.

Chittajallu, R., Chen, Y., Wang, H., Yuan, X., Ghiani, C.A., Heckman, T., McBain, C.J., Gallo, V. (2002) Regulation of Kv1 subunit expression in oligodendrocyte progenitor cells and their role in G1/S phase progression of the cell cycle. *Proc Natl Acad Sci USA* **99**, 2350-5.

Clark, K.J., Balciunas, D, Pogoda, H.M., Ding, Y., Westcot, S.E., Bedell, V.M., Greenwood, T.M., Urban, M.D., Skuster, K.J., Petzold, A.M. et al. (2011). In vivo protein trapping produces a functional expression codex of the vertebrate proteome. *Nat Methods* **8**, 506-515.

Development • Advance article

Copp, A.J., Greene, N.D., Murdoch, J.N. (2003). The genetic basis of mammalian neurulation. *Nat. Rev. Genet.* **4**, 784–793.

Damkier, H.H., Praetorius, J. (2012) Genetic ablation of Slc4a10 alters the expression pattern of transporters involved in solute movement in the mouse choroid plexus. *Am. J. Physiol. Cell Physiol.* **302**, C1452-9.

David JP, Stas JI, Schmitt N, Bocksteins E. (2015) Auxiliary KCNE subunits modulate both homotetrameric Kv2.1 and heterotetrameric Kv2.1/Kv6.4 channels. *Sci. Rep.* **5**,12813.

Deng, X.L., Lau, C.P., Lai, K., Cheung, K.F., Lau, G.K., Li, G.R. (2007) Cell cycle-dependent expression of potassium channels and cell proliferation in rat mesenchymal stem cells from bone marrow. *Cell Prolif.* **40**, 656-670.

Du, J., Haak, L.L., Phillips-Tansey, E., Russell, J.T., McBain, C.J. (2000) Frequency-dependent regulation of rat hippocampal somato-dendritic excitability by the K+ channel subunit Kv2.1. *J. Physiol.* **522**,19-31.

Feinshreiber, L., Singer-Lahat, D., Ashery, U., Lotan, I. (2009) Voltage-gated potassium channel as a facilitator of exocytosis. *Ann. N Y Acad. Sci.* **1152**, 87-92.

Feinshreiber, L., Singer-Lahat, D., Friedrich, R., Matti, U., Sheinin, A., Yizhar, O., Nachman, R., Chikvashvili, D., Rettig, J., Ashery, U., et al. (2010) Non-conducting function of the Kv2.1 channel enables it to recruit vesicles for release in neuroendocrine and nerve cells. *J. Cell Sci.* **123**, 1940-7.

Fossan G, Cavanagh ME, Evans CA, Malinowska DH, Møllgård K, Reynolds ML, Saunders NR. (1985) CSF-brain permeability in the immature sheep fetus: a CSF-brain barrier. *Brain Res* **350**, 113-24.

Garcia-Lecea, M., Kondrychyn, I., Fong, S.H., Ye, Z.R., Korzh, V. (2008). In vivo analysis of choroid plexus morphogenesis in zebrafish. *PloS One* **3**, e3090.

Development • Advance article

Green, A.L., Pereira, E.A., Kelly, D., Richards, P.G., Pike, M.G. (2007) The changing face of paediatric hydrocephalus: a decade's experience. *J. Clin. Neurosci.* **14**, 1049-54.

Gu, Y., Rosenblatt, J. (2012) New emerging roles for epithelial cell extrusion. *Curr. Opin. Cell Biol.* **24**, 865-70.

Guo, Y., Ma, L., Cristofanilli, M., Hart, R.P., Hao, A., Schachner, M. (2011) Transcription factor Sox11b is involved in spinal cord regeneration in adult zebrafish. *Neuroscience* **172**, 329-41.

Gutman, G.A., Chandy, K.G., Grissmer, S., Lazdunski, M., McKinnon, D., Pardo, L.A., Robertson, G.A., Rudy, B., Sanguinetti, M.C., Stühmer, W., et al. (2005) International Union of Pharmacology. LIII. Nomenclature and molecular relationships of voltage-gated potassium channels. *Pharmacol. Rev.* **57**, 473-508.

Gutzman, J.H., Sive, H. (2010). Epithelial relaxation mediated by the myosin phosphatase regulator Mypt1 is required for brain ventricle lumen expansion and hindbrain morphogenesis. *Development* **137**, 795-804.

Hamilton, L.K., Truong, M.K., Bednarczyk, M.R., Aumont, A., Fernandes, K.J. (2009) Cellular organization of the central canal ependymal zone, a niche of latent neural stem cells in the adult mammalian spinal cord. *Neuroscience* **164**, 1044-56.

Harris, M.J., Juriloff, D.M. (2010). An update to the list of mouse mutants with neural tube closure defects and advances toward a complete genetic perspective of neural tube closure. *Birth Defects Res. Part A Clin. Mol. Teratol.* **88**, 653–669.

Hwang, W.Y., Fu, Y., Reyon, D., Maeder, M.L., Tsai, S.Q., Sander, J.D., Peterson, R.T., Yeh, J.R., Joung, J.K. (2013) Efficient genome editing in zebrafish using a CRISPR-Cas system. *Nature Biotech* **31**, 227-229.

Development • Advance article

Jiménez AJ, Tomé M, Páez P, Wagner C, Rodríguez S, Fernández-Llebrez P, Rodríguez EM, Pérez-Fígares JM. (2001) A programmed ependymal denudation precedes congenital hydrocephalus in the hyh mutant mouse. *J Neuropathol Exp Neurol* **60**, 1105-19.

Johanson, C. (2003) The Choroid Plexus–CSF Nexus. Gateway to the Brain. In: Michael Conn P, ed. Neuroscience in Medicine. Totowa, NJ: Humana Press Inc. pp. 165–195.

Johansson, C.B., Svensson, M., Wallstedt, L., Janson, A.M., Frisén, J. (1999) Neural stem cells in the adult human brain. *Exp. Cell Res.* **253**, 733-6.

Kimmel, C.B., Ballard, W.W., Kimmel, S.R., Ullmann, B., Schilling, T.F. (1995). Stages of embryonic development of the zebrafish. *Dev. Dynam.* **203**, 253-310.

Kondrychyn, I., Teh, C., Sin, M., Korzh, V. (2013). Stretching morphogenesis of the roof plate and formation of the central canal. *PloS One* **8**, e56219.

Korzh, V., Sleptsova-Friedrich, I., Liao, J., He, J., Gong, Z. (1998). Expression of zebrafish bHLH genes *ngn1* and *nrD* define distinct stages of neural differentiation. *Dev. Dynam.* **213**, 92-104

Korzh, V. (2014) Stretching cell morphogenesis during late neurulation and mild neural tube defects. *Dev. Growth Differ.* **56**, 425-33.

Lein, E.S., Hawrylycz, M.J., Ao, N., Ayres, M., Bensinger, A., Bernard, A., Boe, A.F., Boguski, M.S., Brockway, K.S., Byrnes, E.J, et al. (2007) Genome-wide atlas of gene expression in the adult mouse brain. *Nature* **445**, 168-76.

Liu, Y.G., and Whittier, R.F. (1995). Thermal asymmetric interlaced PCR: automatable amplification and sequencing of insert end fragments from P1 and YAC clones for chromosome walking. *Genomics* **25**, 674-681.

Development • Advance article

Leung, L., Klopper, A.V., Grill, S.W., Harris, W.A., Norden, C. (2011). Apical migration of nuclei during G2 is a prerequisite for all nuclear motion in zebrafish neuroepithelia. *Development* **138**, 5003-5013.

Li, T., Jiang, L., Chen, H., Zhang, X. (2008) Characterization of excitability and voltage-gated ion channels of neural progenitor cells in rat hippocampus. *J. Mol. Neurosci.* **35**, 289-95.

Liebau, S., Pröpper, C., Böckers, T., Lehmann-Horn, F., Storch, A., Grissmer, S., Wittekindt, O.H. (2006) Selective blockage of Kv1.3 and Kv3.1 channels increases neural progenitor cell proliferation. *J. Neurochem.* **99**, 426-37.

Long, S.B., Campbell, E.B., Mackinnon, R. (2005) Crystal structure of a mammalian voltage-dependent Shaker family K+ channel. *Science* **309**, 897-903.

Lowery, L.A., and Sive, H. (2005). Initial formation of zebrafish brain ventricles occurs independently of circulation and requires the nagie oko and snakehead/atp1a1a.1 gene products. *Development* **132**, 2057-2067.

Meletis, K., Barnabé-Heider, F., Carlén, M., Evergren, E., Tomilin, N., Shupliakov, O., Frisén, J. (2008). Spinal cord injury reveals multilineage differentiation of ependymal cells. *PLoS Biol.* **6**, e182.

Merkle, F.T., Alvarez-Buylla, A. (2006). Neural stem cells in mammalian development. *Curr. Opin. Cell Biol.* **18**, 704-709.

Mirzadeh, Z., Merkle, F.T., Soriano-Navarro, M., Garcia-Verdugo, J.M., Alvarez-Buylla, A. (2008) Neural stem cells confer unique pinwheel architecture to the ventricular surface in neurogenic regions of the adult brain. *Cell Stem Cell* **3**, 265-78.

Muller, D,, Cherukuri, P,, Henningfeld, K., Poh, C.H., Wittler, L., Grote, P., Schluter, O., Schmidt, J., Laborda, J., Bauer, SR et al. (2014). Dlk1 promotes a fast motor

Development • Advance article

neuron biophysical signature required for peak force execution. *Science* **343**, 1264-1266.

Munson, C., Huisken, J., Bit-Avragim, N., Kuo, T., Dong, P.D., Ober, E.A., Verkade, H., Abdelilah-Seyfried, S., Stainier, D.Y. (2008) Regulation of neurocoel morphogenesis by Pard6 gamma b. *Dev. Biol.* **324**, 41-54.

Murakoshi, H., Trimmer, J.S. (1999) Identification of the Kv2.1 K+ channel as a major component of the delayed rectifier K+ current in rat hippocampal neurons. *J. Neurosci.* **19**,1728-35.

Ottschytsch, N., Raes, A., Van Hoorick, D., Snyders, D.J. (2002). Obligatory heterotetramerization of three previously uncharacterized Kv channel alpha-subunits identified in the human genome. *Proc. Nat. Acad. Sci. USA* **99**,7986-7991.

Ottschytsch, N., Raes, A.L., Timmermans, J.P., Snyders, D.J. (2005) Domain analysis of Kv6.3, an electrically silent channel. *J. Physiol* **568**, 737-747.

Pardo, L.A. (2004). Voltage-gated potassium channels in cell proliferation. *Physiology* **19**, 285-292.

Parinov, S., Kondrichin, I., Korzh, V., Emelyanov, A. (2004). Tol2 transposon mediated enhancer trap to identify developmentally regulated zebrafish genes in vivo. *Dev. Dynam.* **231**, 449-459.

Rosenblatt, J., Raff, M.C., Cramer,L.P. (2001) An epithelial cell destined for apoptosis signals its neighbors to extrude it by an actin- and myosin-dependent mechanism. *Curr. Biol.* **11**,1847-57.

Sakka, L., Coll, G., Chazal, J. (2011) Anatomy and physiology of cerebrospinal fluid. *Eur. Ann. Otorhinolaryngol. Head Neck Dis.* **128**, 309-316.

Sivasubbu, S., Balciunas, D., Amsterdam, A., Ekker, S.C. (2007). Insertional mutagenesis strategies in zebrafish. *Genome Biol.* **8** Suppl 1, S9.

Development • Advance article

Sivasubbu, S., Balciunas, D., Davidson, A.E., Pickart, M.A., Hermanson, S.B., Wangensteen, K.J., Wolbrink, D.C., Ekker, S.C. (2006). Gene-breaking transposon mutagenesis reveals an essential role for histone H2afza in zebrafish larval development. *Mech Dev.* **123,** 513-529.

Skjolding, A.D., Holst, A.V., Broholm, H., Laursen, H., Juhler, M. (2013). Differences in distribution and regulation of astrocytic aquaporin-4 in human and rat hydrocephalic brain. *Neuropathol. Appl. Neurobiol.* **39**,179-191.

Smith, D.O., Rosenheimer, J.L., Kalil, R.E. (2008). Delayed rectifier and A-type potassium channels associated with Kv2.1 and Kv4.3 expression in embryonic rat neural progenitor cells. *PloS One* **3**, e1604.

Thorneloe, K.S., Nelson, M.T. (2003). Properties and molecular basis of the mouse urinary bladder voltage-gated K+ current. *J Physiol.* **549**, 65-74.

Tully, H.M., Dobyns, W.B. (2014) Infantile hydrocephalus: a review of epidemiology, classification and causes. *Eur. J. Med. Genet.* **57**, 359-68.

Vacher, H., Mohapatra, D.P., Trimmer, J.S. (2008). Localization and targeting of voltage-dependent ion channels in mammalian central neurons. *Physiol Rev* **88**, 1407-1447.

Whish S, Dziegielewska KM, Møllgård K, Noor NM, Liddelow SA, Habgood MD, Richardson SJ, Saunders NR. (2015) The inner CSF-brain barrier: developmentally controlled access to the brain via intercellular junctions. *Front Neurosci* **12**, 16.

Wonderlin, W.F., Strobl, J.S. (1996). Potassium channels, proliferation and G1 progression. *J. Membrane Biol.* **154**, 91-107.

Zhang, J., Williams, M.A., Rigamonti, D. (2006) Genetics of human hydrocephalus. *J. Neurol.* **253**, 1255-66.

Development • Advance article

Figures:

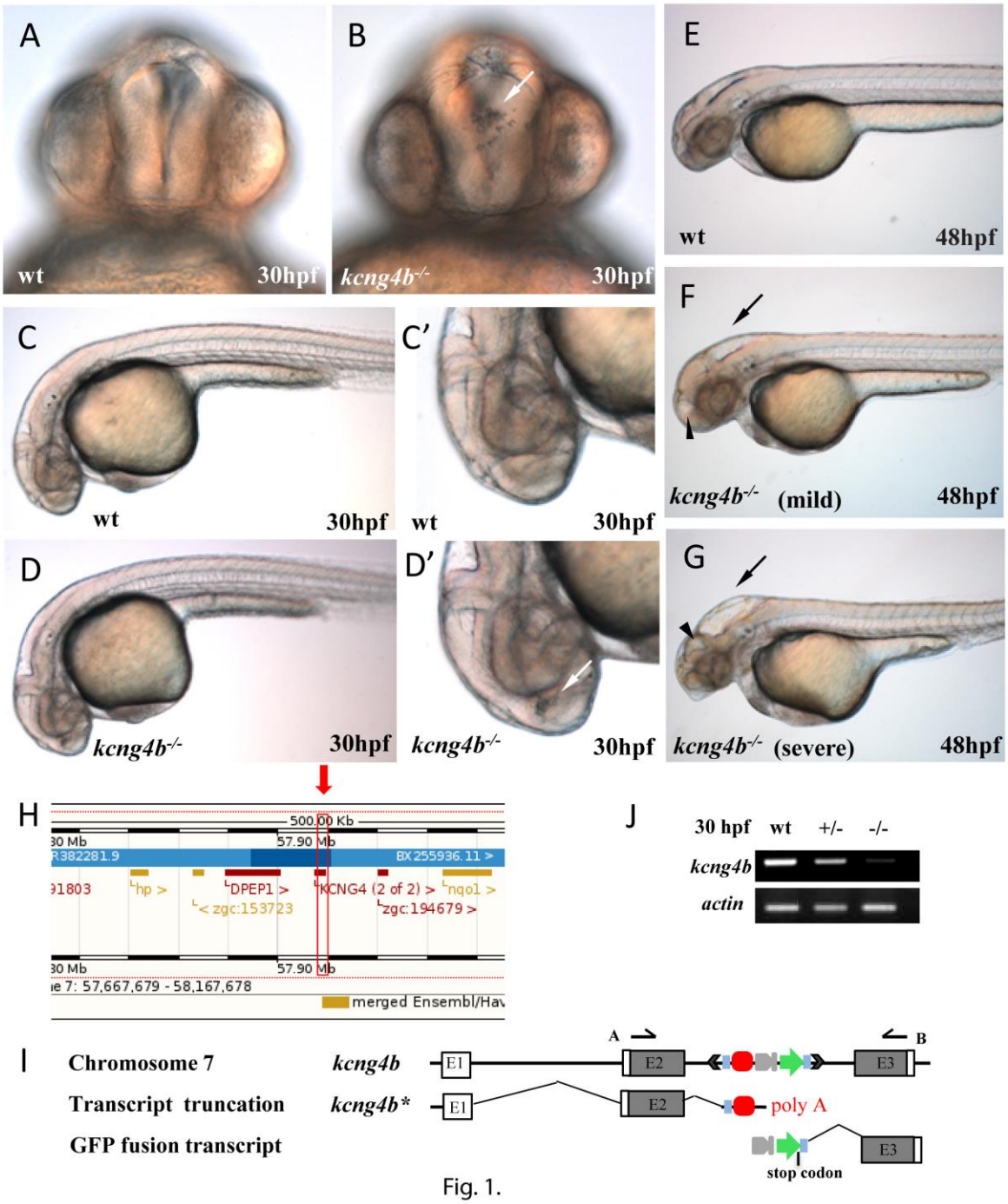

Fig. 1.

Fig. 1. Insertion of the GBT cassette into the second intron of *kcng4b* causes a mutation.

(A-D) Homozygous mutants show a clump of cells in the third ventricle (30 hpf-B,D,D', white arrow) and hydrocephalus (48 hpf-F,G, black arrow and arrowheads). (H) TAIL-PCR

Development • Advance article

mapped the insertion at position 57,917,547 on Chr. 7, in (+) orientation (Zv9). (I) Insertion into the *kcng4b* locus truncates the full-length transcript. *kcng4b*$^{-/-}$ expresses the truncated transcript - *kcng4b** consisting of one coding exon. (J) RT-PCR analysis demonstrated reduction of *kcng4b* transcripts in *kcng4b*$^{+/-}$ and their absence in *kcng4b*$^{-/-}$ (30 hpf). *actin* - loading control. (A,B) frontal views, (C-G) lateral views, anterior to the left.

Abbreviations:, e – exon, h – hours post fertilization, wt – wild type.

Development • Advance article

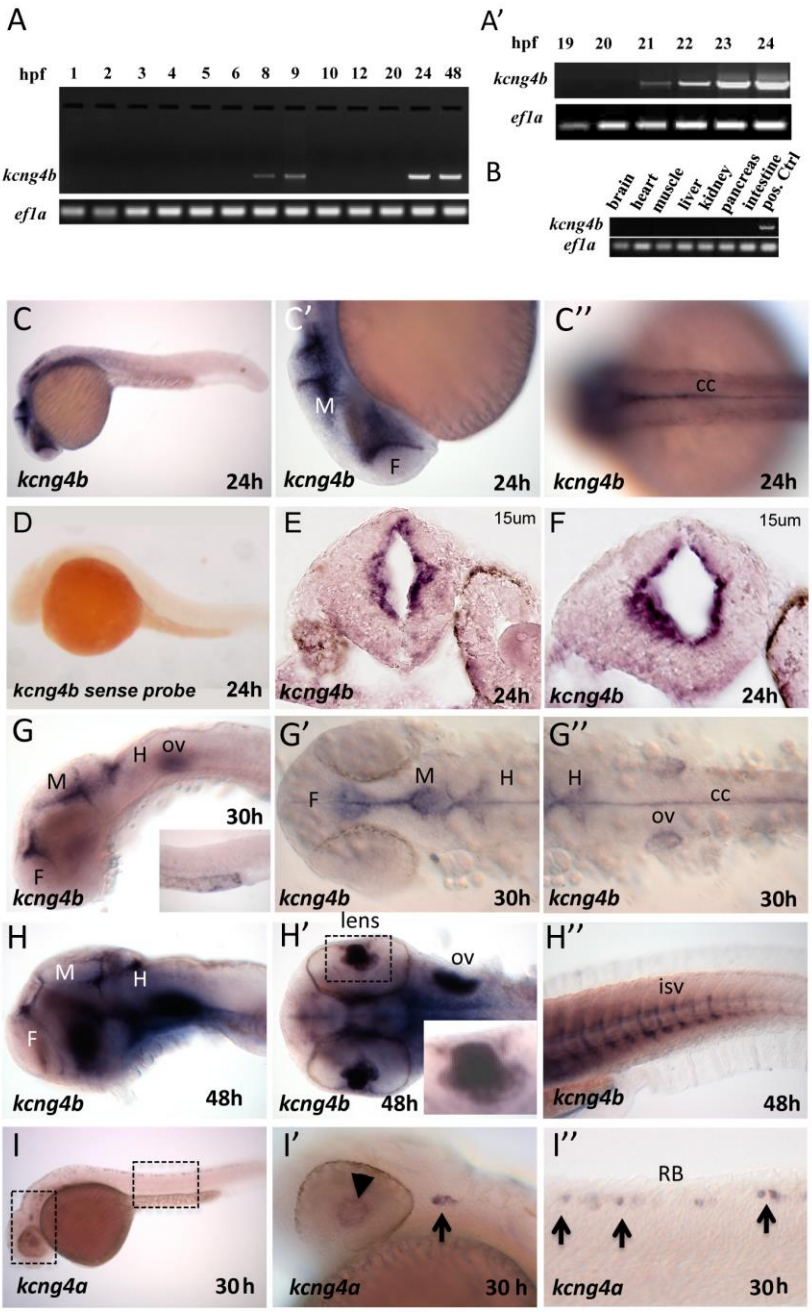

Fig. 2.

Fig. 2. *kcng4b* expression was detected by RT-PCR in embryos (A), but not in adults (B). (C) Antisense WISH detected expression of *kcng4b* in the ventricular zone (24 hpf). C', blowup, lateral view. C'', blowup of the spinal cord, dorsal view. (D) *kcng4b* sense probe detected no signal. (E, F) Two transverse cryosections (15μm, oblique, midbrain). (G, H) 30-

Development • Advance article

48hpf, *kcng4b* transcripts in the ventricular system, otic vesicle (G'', H'), anterior and posterior eye chambers, lenses (H'), and in intersegmental vessels (H''). (G, H), eyes removed, (G',G''), flatmount with yolk removed. (H') inset, lens, including blowup. (I) *kcng4a* transcripts in sensory neurons and lens, 30 hpf. (I') blowup - the head (box) with lens (arrowhead) and trigeminal ganglion (arrow). (I'') blowup - the spinal cord (box), sensory Rohon-Beard neurons (arrows). Abbreviations here and elsewhere: cc, central canal; h, hindbrain; f, forebrain; isv, intersegmental vessels; m, midbrain; mhb, midbrain-hindbrain boundary; ov, otic vesicle; rb, Rohon-Beard neurons.

Development • Advance article

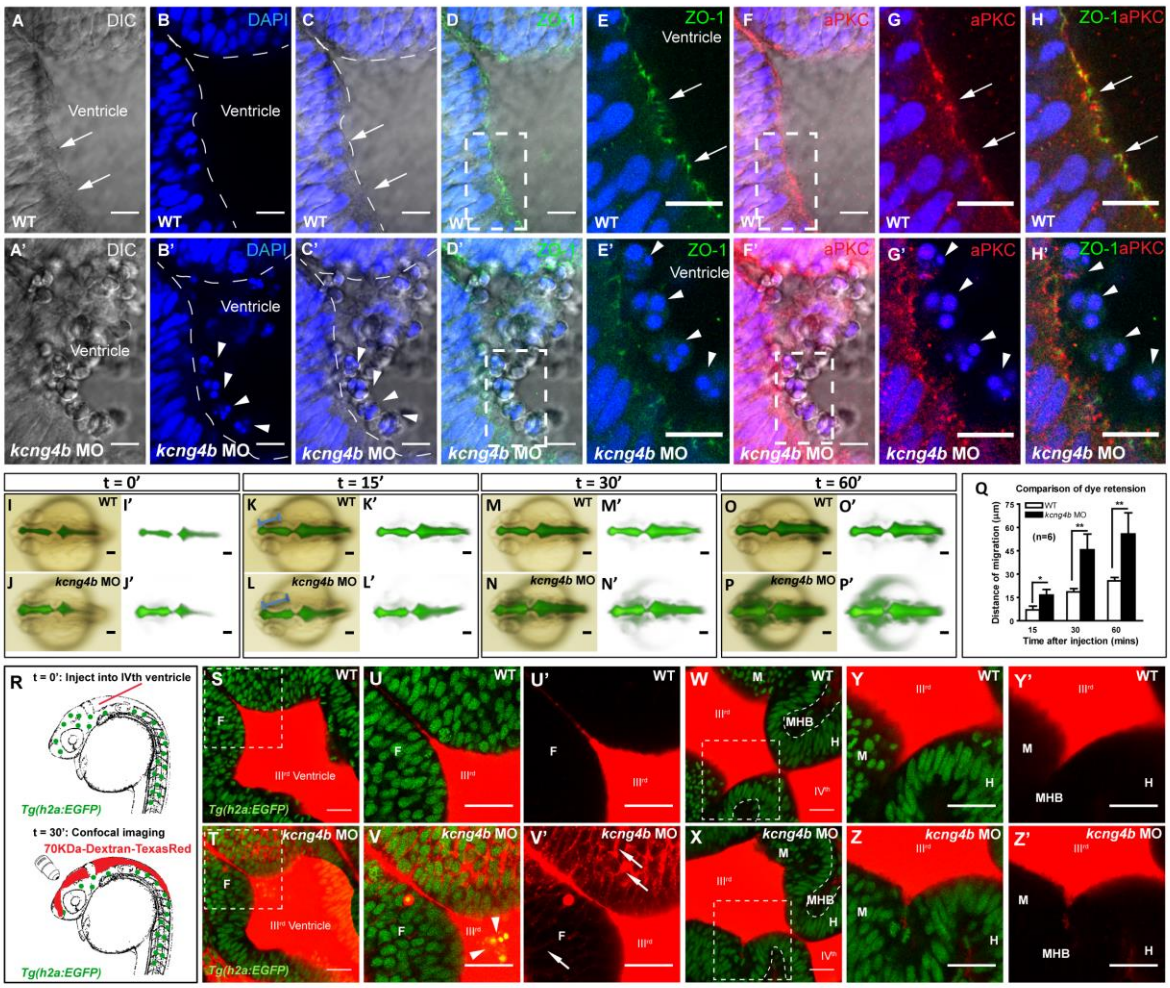

Fig. 3.

Fig. 3. Analyses of tissue integrity. (A-H) Confocal sections (dorsal view), in the upper left corner the anterior portion of third ventricle. Controls (A-H) and *kcng4b* morphants (A'-H'). In the control the apical membrane (arrow) is continuous (A), and in the morphants discontinuous with cells in the ventricular cavity (A'). (B'-C') DAPI stains cell nuclei (arrowhead) in the ventricular lumen (dashed line) of *kcng4b* mutants. (D-H) Apical markers ZO-1 (green, D', E') and aPKC (red, F',G') clearly define plasma membrane in controls, but not in *kcng4b* morphants. (E,E',G,G') blowups of boxed areas in D and F, respectively. H, merged E and G. 63X-water dipping objective on wholemount 24 hpf embryos (dorsal view). Scale bar (A-H): 10 µm.

Development • Advance article

(I-P) Dye retention assay. (I-O) and *kcng4b* mutant (J-P) embryos (24 hpf). Scale bar (I-P): 10 μm. (Q) Dye leakage was quantified by measuring an extent of migration of the dye front along a blue line in K and L. Each time point represents an average of data from six independent experiments. Error bar: SEM, Statistical analysis: unpaired t test, *: $p < 0.05$, **: $p < 0.01$ as compared to control. (R) Confocal analysis of 70KDa-Dextran leakage after injection into IVth ventricle. (S-Z) Confocal section (dorsal view) of neuroepithelium 30' after dye injection into wild-type and *kcng4b* MO embryo in *Tg(h2b:EGFP)* background at 24 hpf. Dye in forebrain neuroepithelium of *kcng4b* MO embryos (arrowed in V,V') (arrowhead in V - delaminated cells) but not in midbrain and hindbrain neuroepithelium (X, Z). U,V, and Y,Z are blowups of boxed areas in S,T and W,X, respectively. Scale bar (S-Z): 25 μm.

Development • Advance article

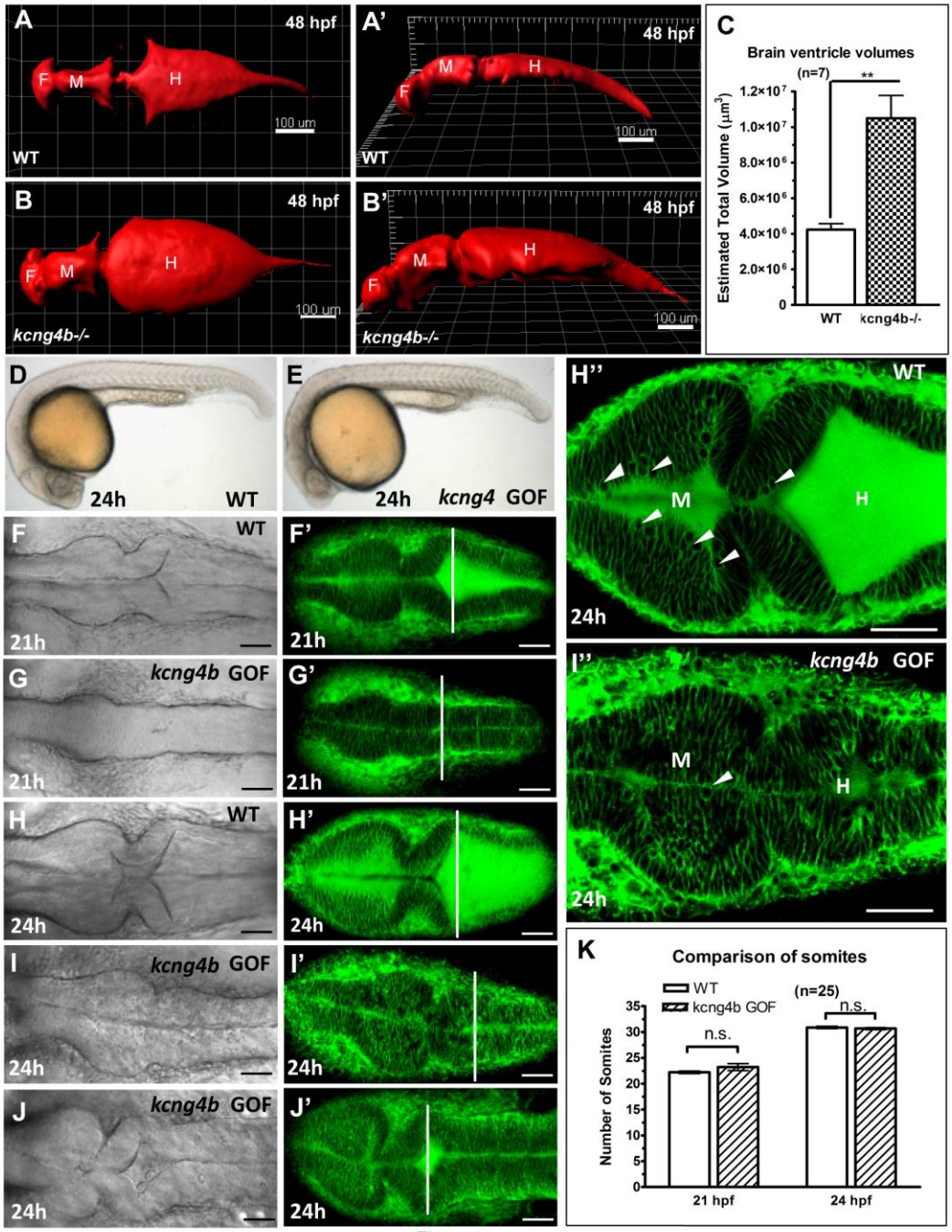

Fig. 4.

Fig. 4. Kcng4b regulates the brain ventricular system. (A,B) 3D-reconstruction of confocal Z-scans of the brain ventricular system *in vivo* after injection with 70kDa-TexasRed-Dextran. A,A', dorsal view. B'B', tilted lateral view. Scale bar: 100μm. (C) Volume measurement of the brain ventricular system by 3D-reconstuction of Z-scans

Development • Advance article

sections using Surface function of Imaris 7.0. Data represents mean with SEM, ** $p < 0.01$, unpaired t-test; scale bar: 100 μm.

(D-J) *kcng4b* GOF 21-24 hpf embryos. D, E, morphology of embryos (lateral view) . F-J, dorsal view of embryos labelled *in vivo* by FITC-BODIPY-ceramide at 21-24 hpf, confocal DIC and maximal projection of Z-scans. The perpendicular line marks the widest opening of the hindbrain ventricle. H'', I'', confocal plane shows the ventricle with BODIPY-labelled cell membranes. Note that the round-shaped cells facing the lumen (arrowhead) are less abundant in *kcng4b* GOF (I'') compared to control (H''). Scale bar (D-J): 50 μm. (K), a number of somites. Error bar: SEM, Statistical analysis: unpaired t-test, n = 25.

Development • Advance article

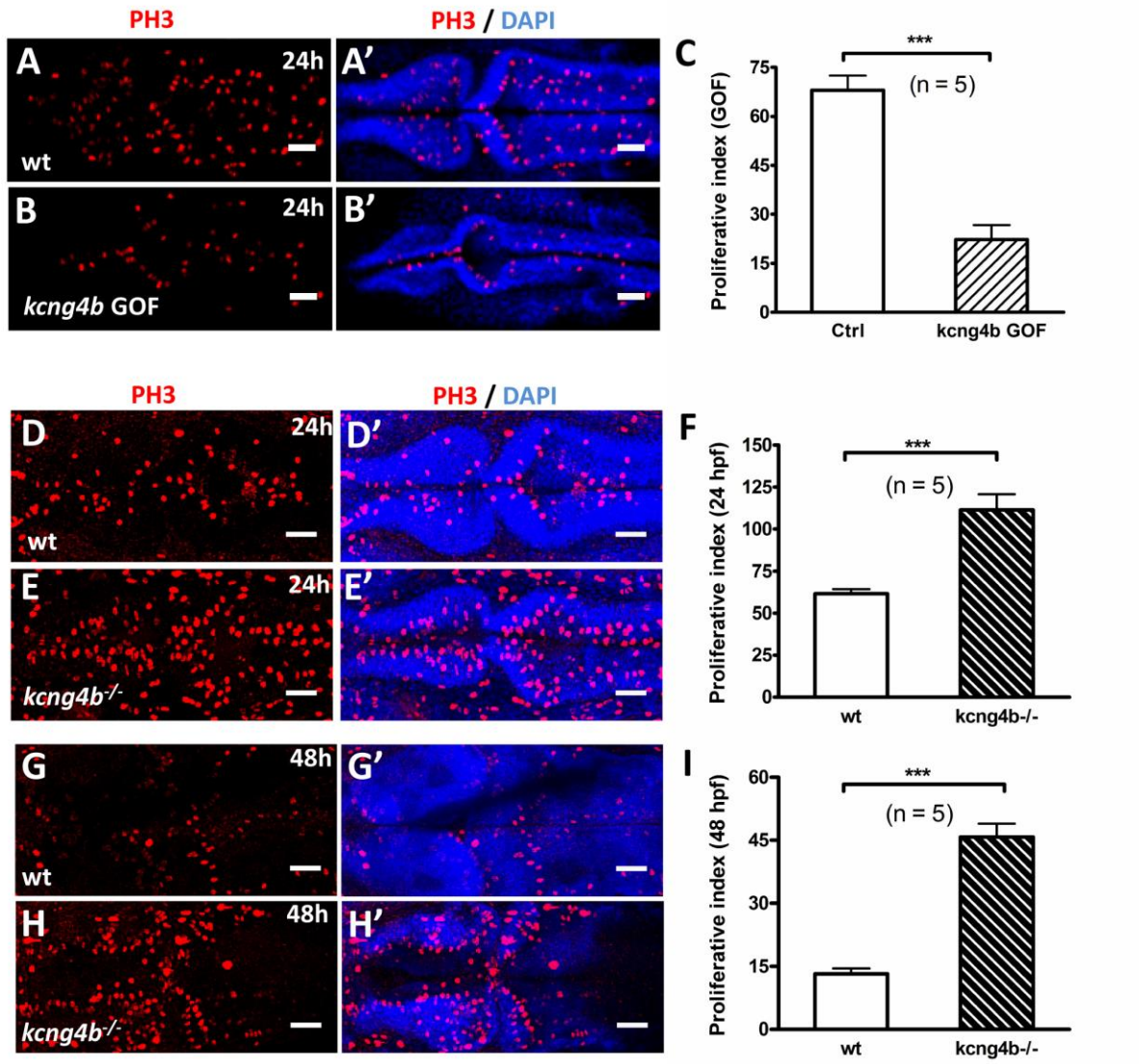

Fig. 5.

Fig. 5. *kcng4b* modulates proliferation in neuroepithelium. (A, B) Confocal projection view of Z-scans of embryos stained for phosphohistone 3 (PH3) and DNA (DAPI) at 24 hpf. Dorsal view, anterior to the left. Scale bar: 50 μm. (C) Proliferative index in control and *kcng4b* GOF embryos. Proliferative index was calculated by counting the number of PH3-positive cells and DAPI-positive neuroepithelial cells of each single confocal optical section

Development • Advance article

using ImageJ cell count function, and expressed as summation of the total number of PH3-positive cells of whole Z-scans per 1000 neuroepithelial cells. ***, $p < 0.001$; unpaired t-test, n = 5. (D-I) Confocal projection view of Z-scans of control and *kcng4b*$^{-/-}$ embryos stained at 24 hpf (D, E) and 48 hpf (G, H). Scale bar: 50 μm. (F, I) Proliferative index in controls and *kcng4b* mutants at same stages. ***, $p < 0.001$; unpaired t-test, n = 5.

Development • Advance article

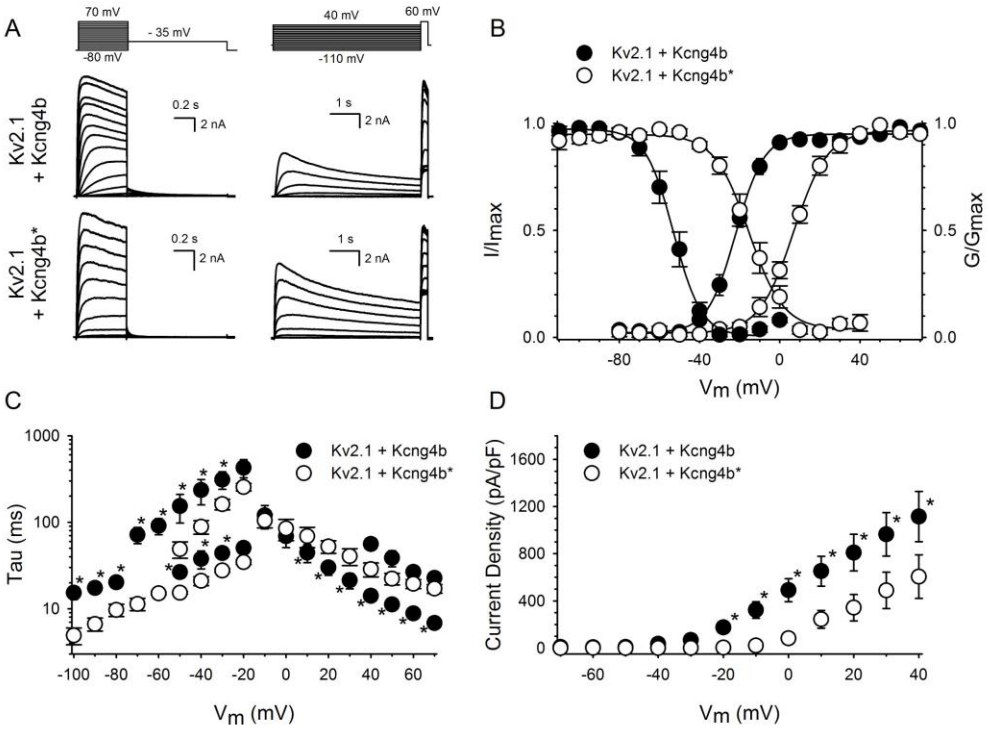

Fig. 6.

Fig. 6. Biophysical properties of Kv2.1 co-expressed with wild type Kcng4b and Kcng4b* in HEK cell line. (A) Representative whole-cell current recordings of Kv2.1 co-expressed with wild-type Kcng4b (upper row) and Kcng4b*(lower row). The activation and inactivation properties were determined from the current recordings in the left and right columns, respectively. The pulse protocols used are shown above. (B) Voltage-dependence of activation and of inactivation. Activation curves were derived by plotting the tail current amplitude at -35 mV as a function of the 500 ms prepulse potential. Inactivation curves were derived by plotting the test pulse amplitude at 60 mV as a function of the 5 sec prepulse potential. Solid lines represent Boltzmann fits. (C) Activation and deactivation time constants

Development • Advance article

determined by fitting the activating and deactivating currents with a single or double exponential function. Note that the Kcng4b* activation time course is characterized by only one component and that the Kcng4b* deactivation time course is accelerated compared to that of Kcng4b (*, $p < 0.05$). (D) Current densities of Kv2.1 upon co-expression with Kcng4b (black symbols) and Kcng4b* (white symbols). Note that co-expression of Kcng4b* reduced the current density compared to Kv2.1 + Kcng4b co-expression. *, significantly different ($p < 0.05$).

Development • Advance article

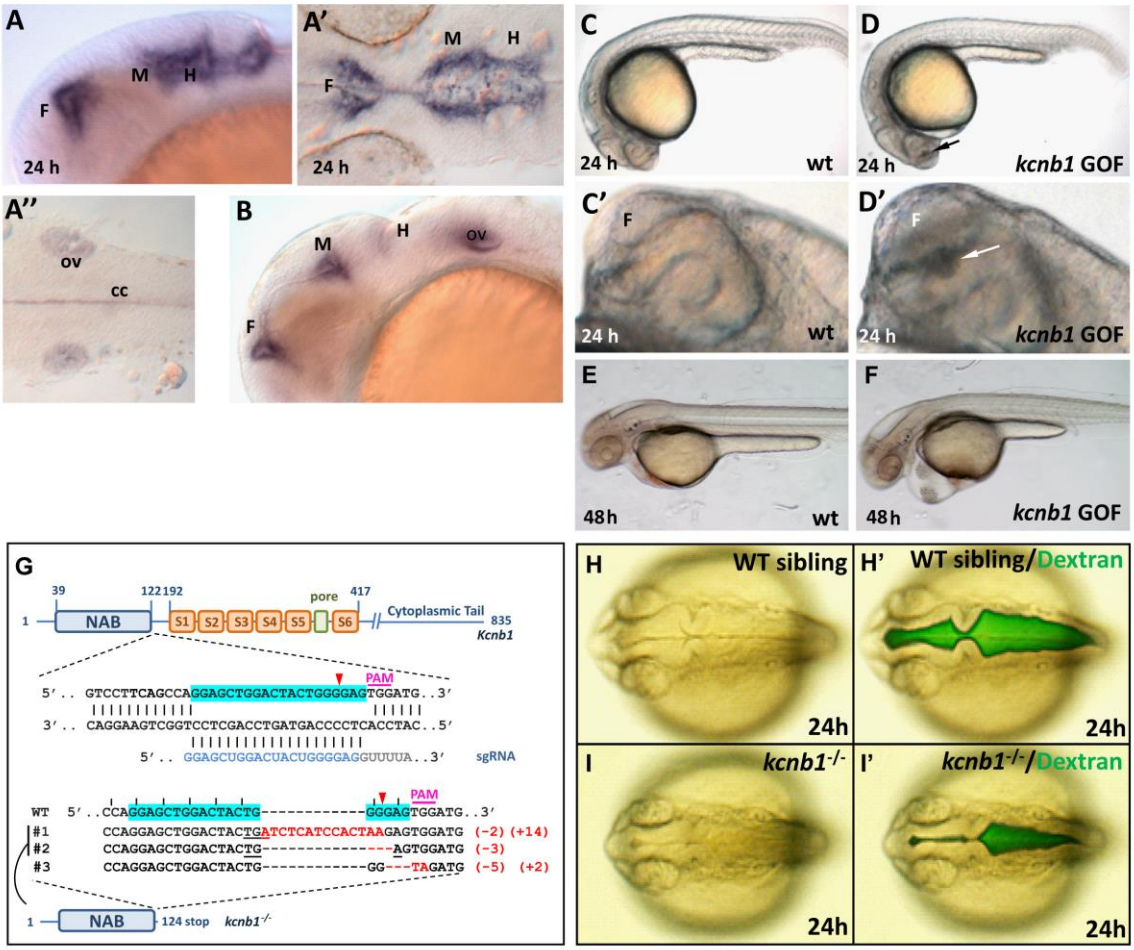

Fig. 7.

Fig. 7. *kcnb1* expressed in the brain similar to *kcng4b*, acts in opposing manner. (A,B) Antisense Dig-RNA WISH detected *kcnb1* transcripts in the ventricular system at 24 and 30 hpf. A, B, lateral view with anterior to the left. A', A'', flat-mount of WISH-stained embryo with anterior to the left. A'', the otic vesicle (ov) and central canal (cc). (C, D) *kcnb1* GOF 24 hpf embryos contain a clump of cells (arrow) in the 3rd ventricle (lateral view, anterior to the left) (C, D). (C',D') blowup of the forebrain with a clump of cells (arrow). (E,F) 48 hpf embryos develop hydrocephalus and cardiac edema. (G) Schematic illustration of *kcnb1* mutant generated using CRISPR-Cas system. Position of the target site, target sequence (blue), single guide RNA (sgRNA) sequence, PAM location (pink), isolated indel mutants

Development • Advance article

(indels in red) and their respective sequences and mutant with truncated *kcnb1* polypeptide are shown. In mutants #1, #2, a premature stop codon (TGA) was found. Mutant #3 is a mis-sense mutant. Mutant #1 was used for all subsequent analysis. (H,I) *kcnb1* LOF results in under-inflated ventricles. H', I', ventricles filled with 70kDa-FITC-dextran. H,I, dorsal view with anterior to the left.

Development • Advance article

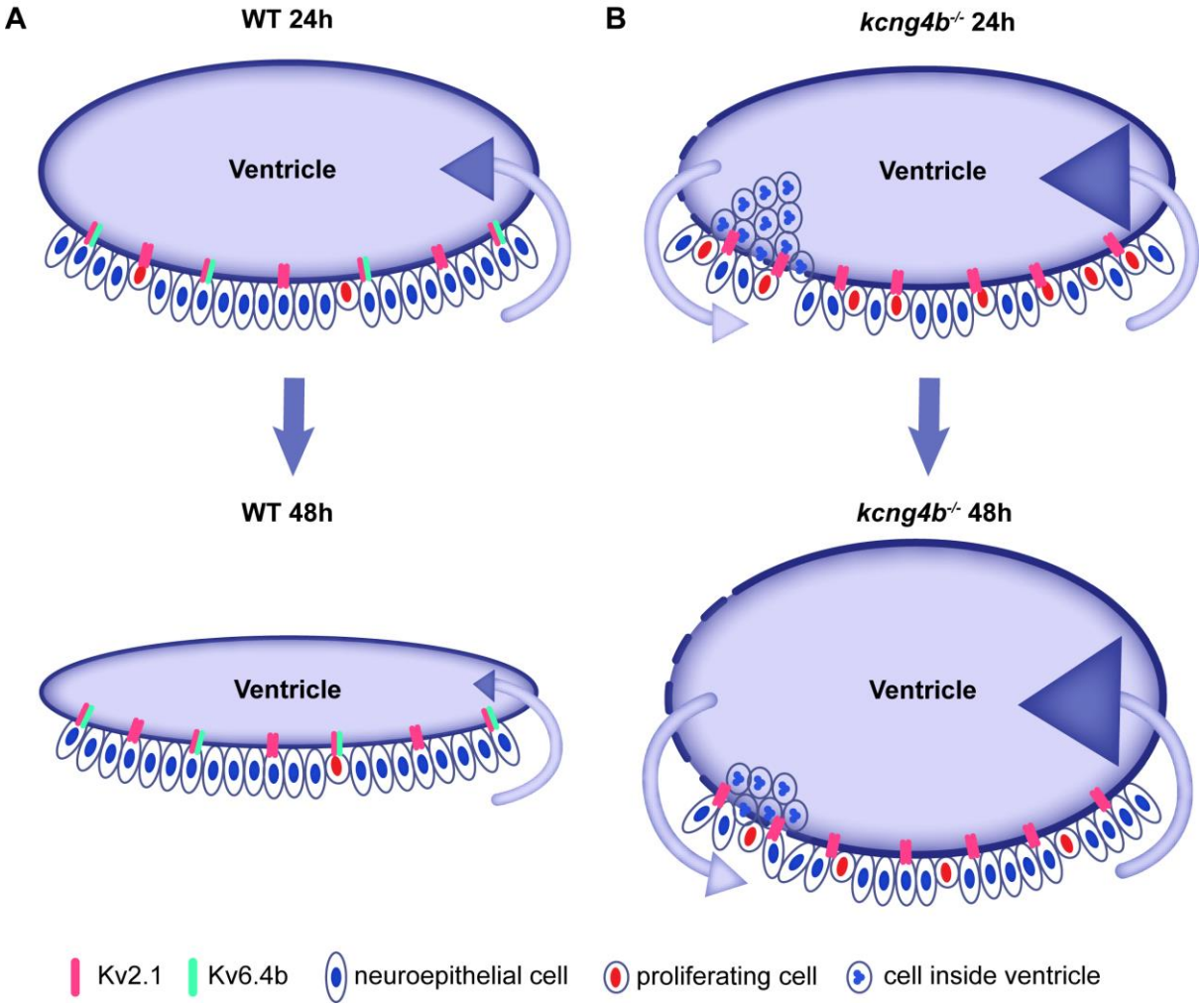

Fig. 8. *kcng4b-kcnb1* establish barrier properties in neuroepithelium of the brain ventricular system. (A) In neuroepithelium of wildtype embryos, Kv6.4b silent subunits (encoded by *kcng4b*) modulate electrically-active Kv2.1 subunits (encoded by *kcnb1*) of the voltage-gated slow-inactivating delayed rectifier (I_K) K channel. Functional antagonism of Kv2.1 and Kv6.4b regulates integrity of neuroepithelium and expansion of the brain ventricular system due to influx of eCSF (arrow, left) and some drainage into surrounding tissues (arrow, right). Cell proliferation leads to filling of the ventricular space from inside by new cells resulting in reduction of ventricular volume by 48 hpf. (B). Loss of Kv6.4b function results in unbalanced increase of Kv2.1 function, hyperproliferation of cells, their

Development • Advance article

extrusion from the neuroepithelial layer and, loss of its integrity. This leads to excessive cells bulging into the brain ventricle, loss of the barrier function and increased influx of eCSF (arrow, left) as well as more drainage into surrounding tissues (arrow, right). Taken together all these processes result in hydrocephalus in the *kcng4b*$^{-/-}$ embryo at 48 hpf.

Development • Advance article

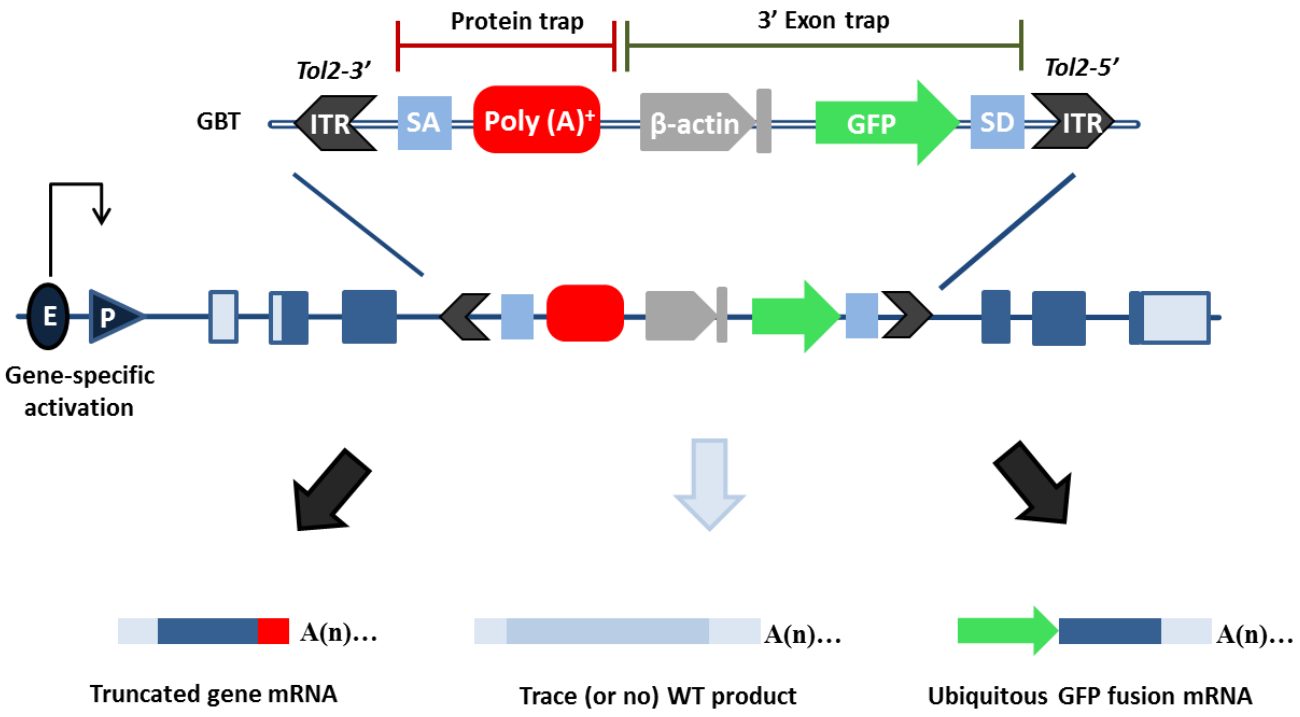

Fig. S1. Schematic representation of the Tol2-mediated GBT vector composed of a protein trap cassette and a 3' exon trap cassette. Insertion of GBT vector (detailed in upper row) into intronic sequence of a gene disrupts native splicing of the gene. The artificial splice donor (SD) and splice acceptor (SA) in the GBT vector fuse with upstream SD and downstream SA, respectively. This results in truncation of the native protein (illustrated in bottom row) Abbreviations: ITR: inverted terminal repeat; SA, splice acceptor: poly(A): polyadenylation signal with extra transcriptional terminator; β-actin: carp beta-actin enhancer and promoter, with noncoding exon and intron 1 sequences; SD, splice donor; E, enhancer; P, promoter.

Development • Supplementary information

A

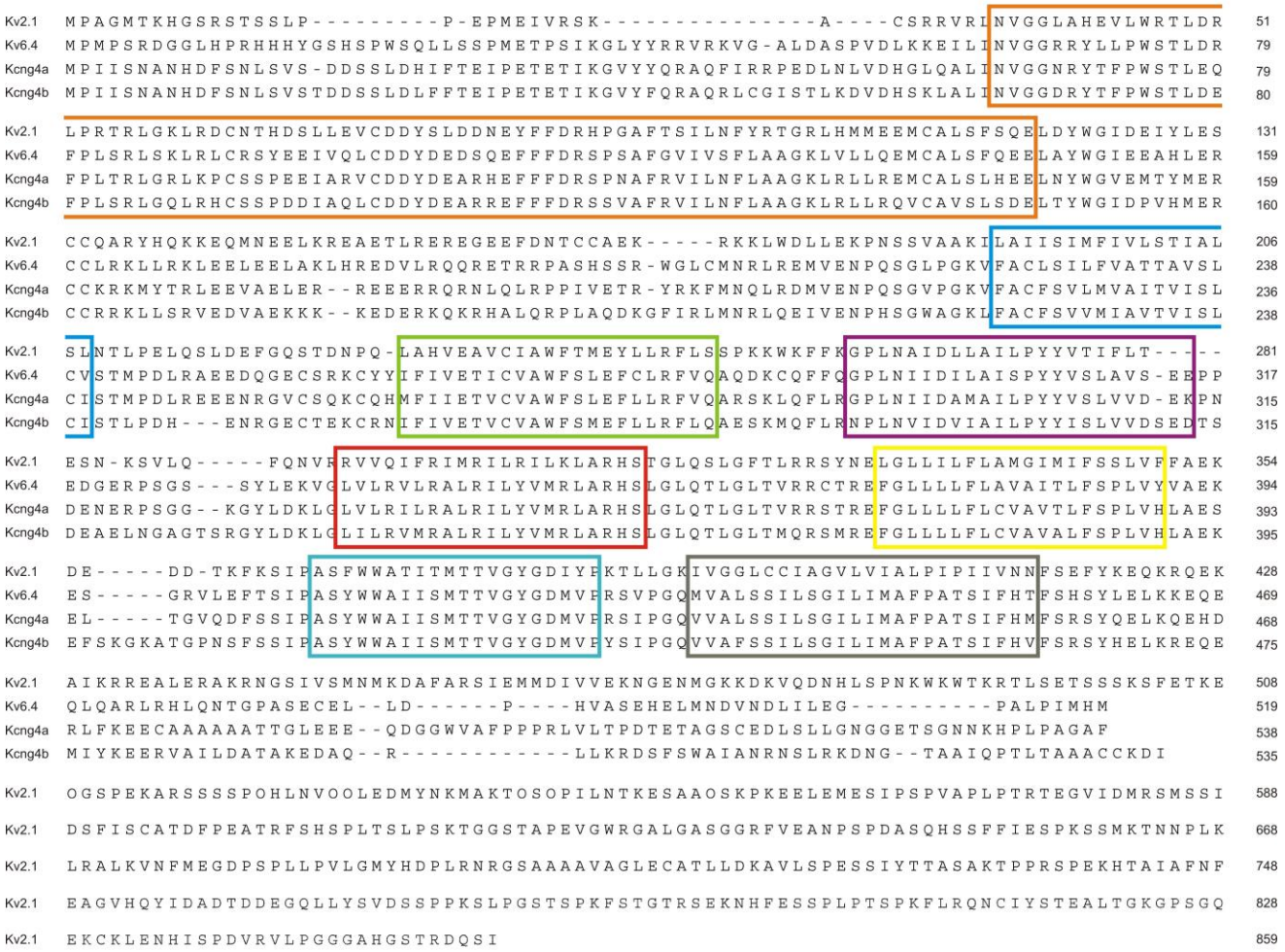

B

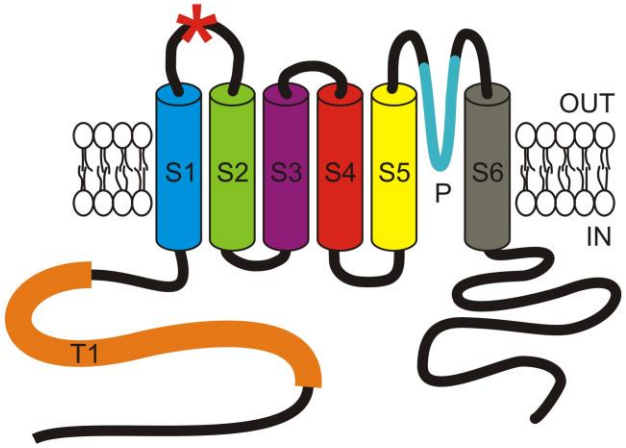

Fig. S2: Kcng4a and Kcng4b demonstrate an evolutionary conservation of the functional domains characteristic for mammalian Shaker-related Kv subunits. (A) Sequence alignment of Kv2.1, Kv6.4, Kcng4a and Kcng4b indicate that Kcng4a and Kcng4b possess all functional domains of a typical Kv subunits. (B) Kv subunits possess a tetramerization domain (T1), six transmembrane segments (S1-S6) with several positively charged residues on S4 and a pore loop (P) containing the K^+ signature sequence GYG. The amino acid sequences that form a specific component of the Kv structure are framed using the same color code as used in the depiction of a Kv subunit represented below the alignment. The red * in the Kv subunit depiction represents the place where the premature termination occurs (at residue R249) in Kcng4b resulting in the Kcng4* mutant that consists of the Kv6.4 N-terminus, S1 segment and a part of the S1-S2 linker.

Development • Supplementary information

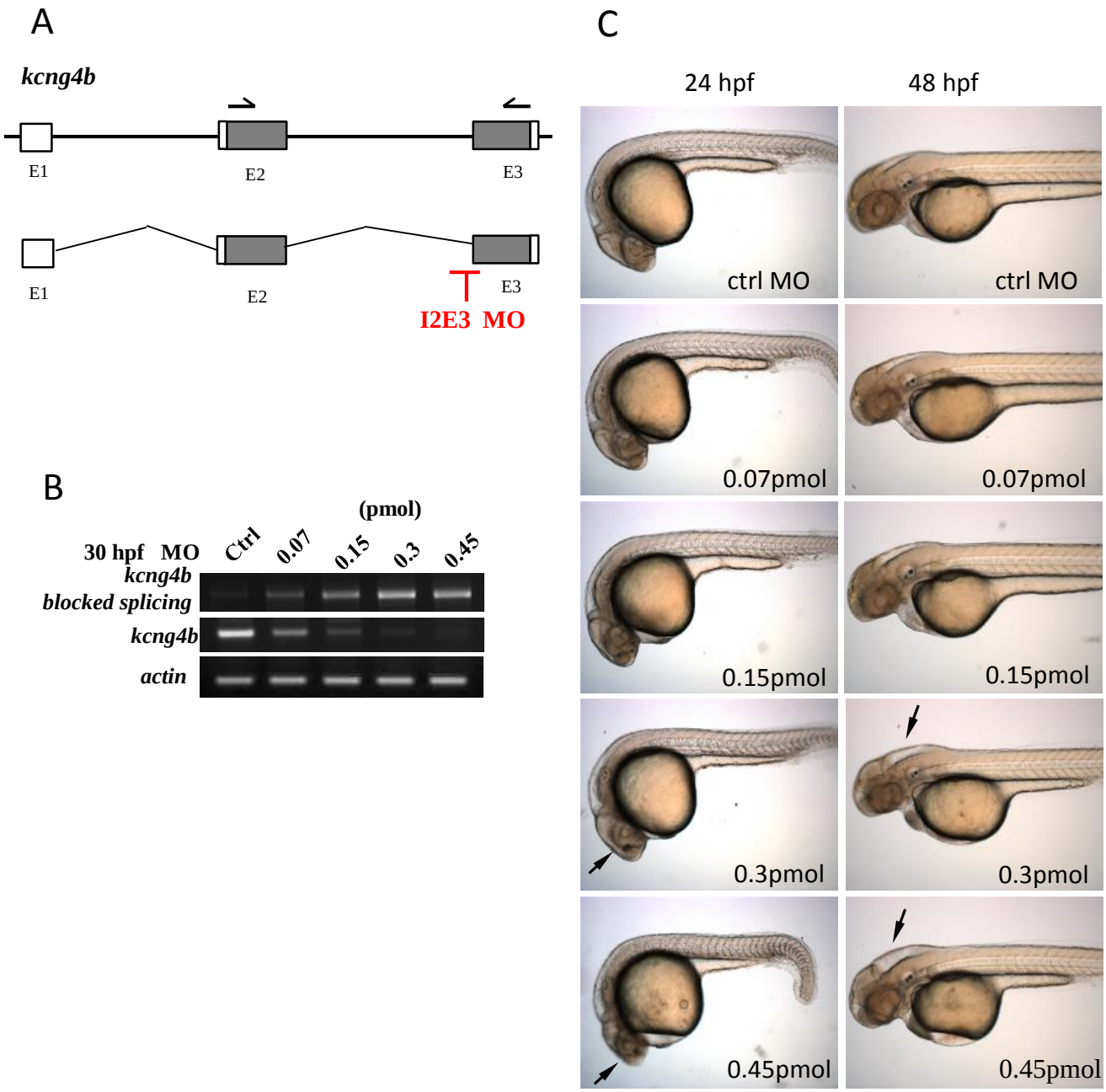

Fig. S3. *kcng4b* splicing morpholino-mediated LOF closely recapitulated the mutant phenotype. (A) The schematics of *kcng4b* organization and the morpholino binding site. The predicted outcome of MO-mediated KD is this case could be very similar to that of mutation, i.e. truncation of the Kcng4 polypeptide after S1 domain. (B) the level of *kcng4b* expression in morphants was reduced in dose-dependent manner. (C) The morphant phenotype closely recapitulates that of the mutant, and the severity of phenotype increased in dose-dependent manner.

Development • Supplementary information

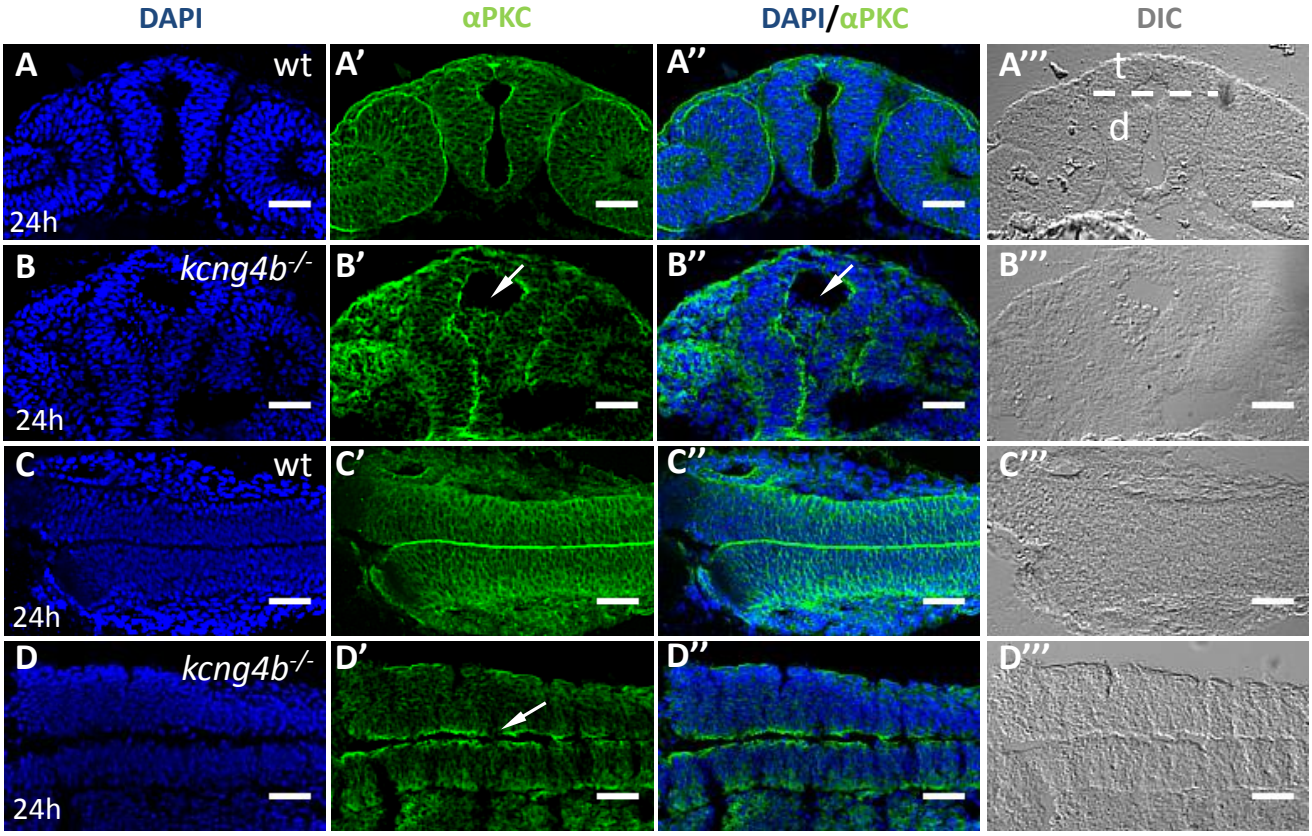

Fig. S4. Loss of Kcng4b disrupts neuroepithelial integrity. (A-D) Confocal image of cross-sections of embryos stained with anti-αPKC antibody (green) and DAPI (blue). A, B, forebrain (cross-section); C,D, hindbrain (tangential section). A,C , controls, B,D, kcng4b -/-. Arrow in B', cells in the ventricle; D', discontinuous labeling. Scale bar: 50 μm.

Development • Supplementary information

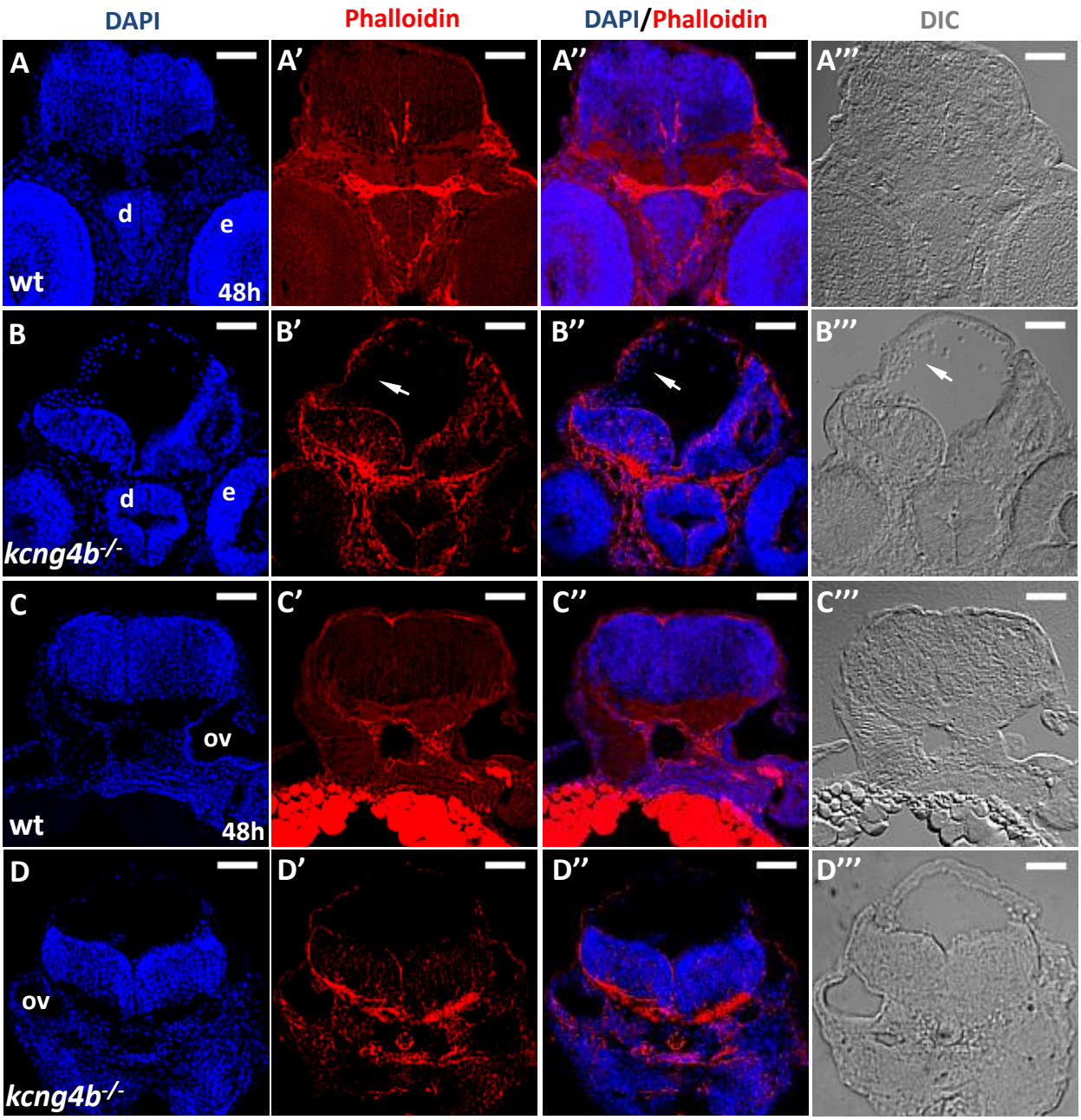

Fig. S5. Apical/basal polarity is affected in cells that dissociated from the ventricular zone in *kcng4b* mutant embryos at 48 hpf. A, B midbrain (cross section near the eyes). C, D – hindbrain (cross section around otic vesicles) A, C – wild-type; B, D – *kcng4b* mutant embryos. Immunostaining by phalloidin (Red), counterstained with DAPI and the same section shown under DIC microscope. Scale bar: 50 μm.

Development • Supplementary information

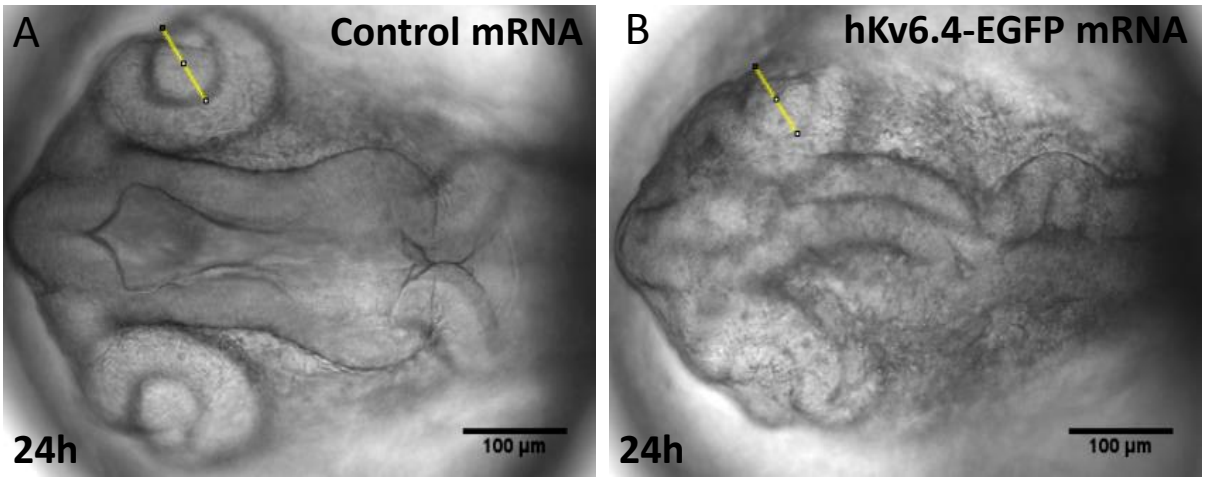

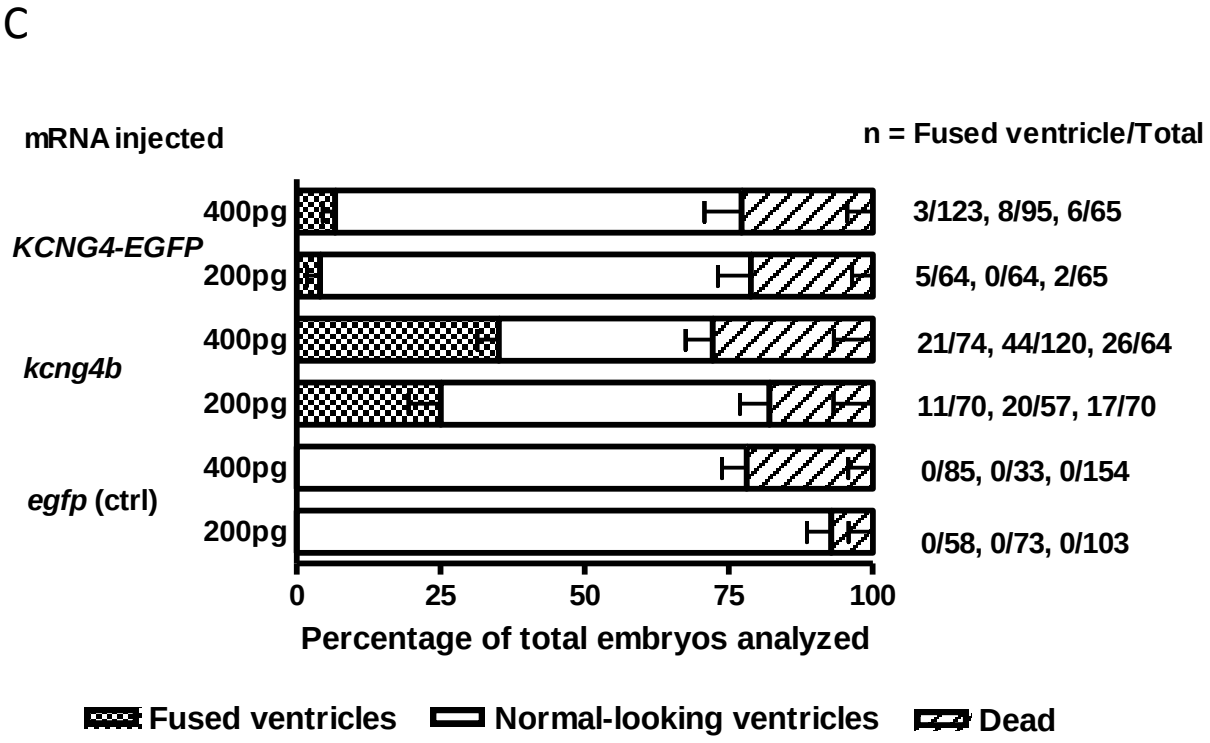

Fig. S6. Overexpression of hkcng4-EGFP in zebrafish embryos blocked ventricle formation. (A, B) Injection of hkcng4-EGFP mRNA into zebrafish embryos caused absence of brain ventricles. Dorsal view of brain ventricle. Scale bar: 100 µm. (C) Comparison of number of embryos with absence of brain ventricles by injection of zebrafish *kcng4b* or hkcng4-EGFP mRNA.

Development • Supplementary information

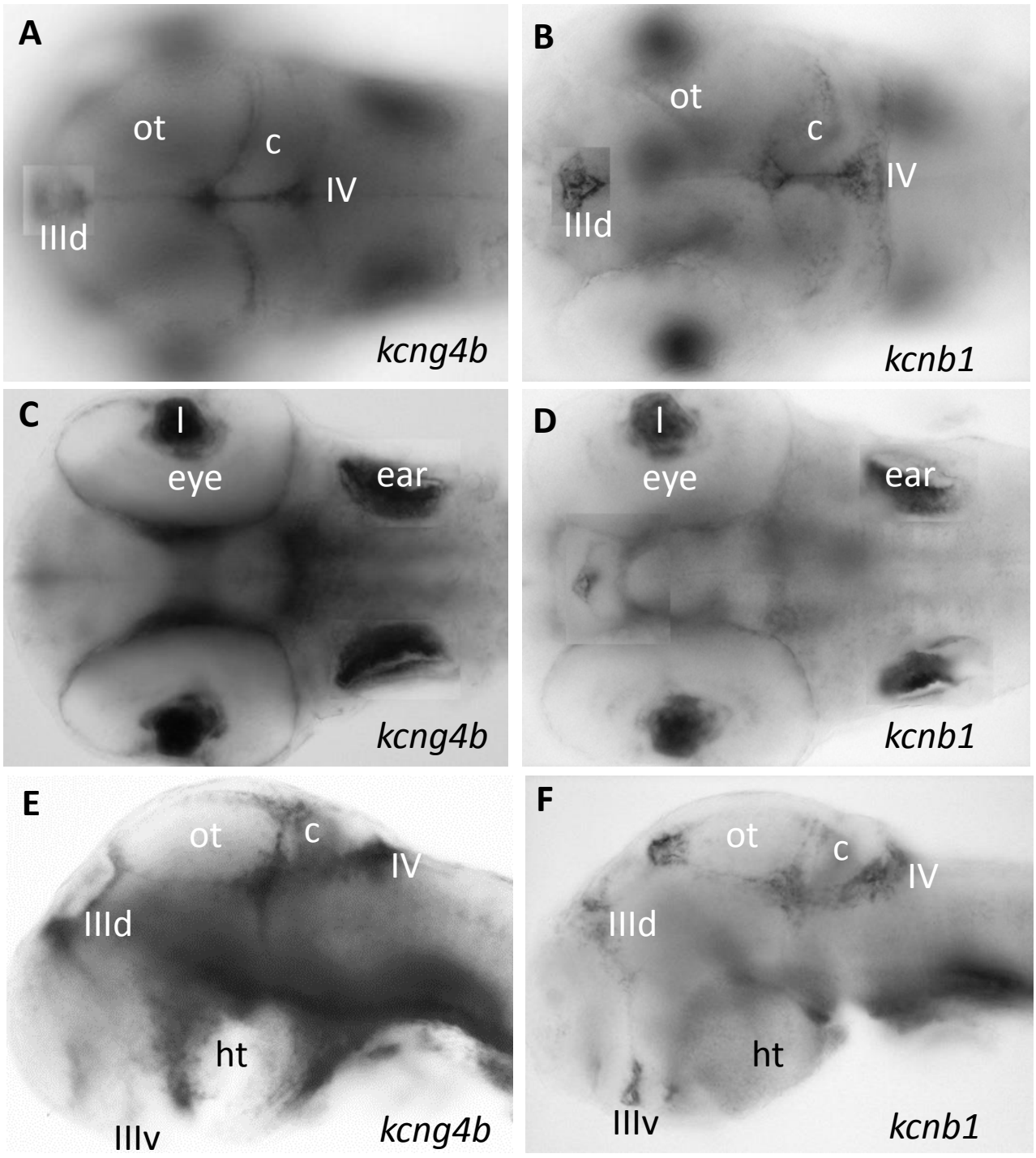

Fig. S7. Similar expression patterns of *kcng4b* and *kcnb1* at 72 hpf. (A-D) Composite images of two optic planes of whole-mount *in situ* hybridization using antisense Dig-labelled RNA probes against *kcng4b* and *kcnb1*. A, B, dorsal planes; C, D, ventral planes. E, F, lateral view after removal of eyes. Abbreviation: c, cerebellum; ht, hypothalamus; l, lens; ot, optic tectum, IIId, dorsal III-rd ventricle; IIIv, ventral III-rd ventricle; IV, IV-th ventricle.

Development • Supplementary information

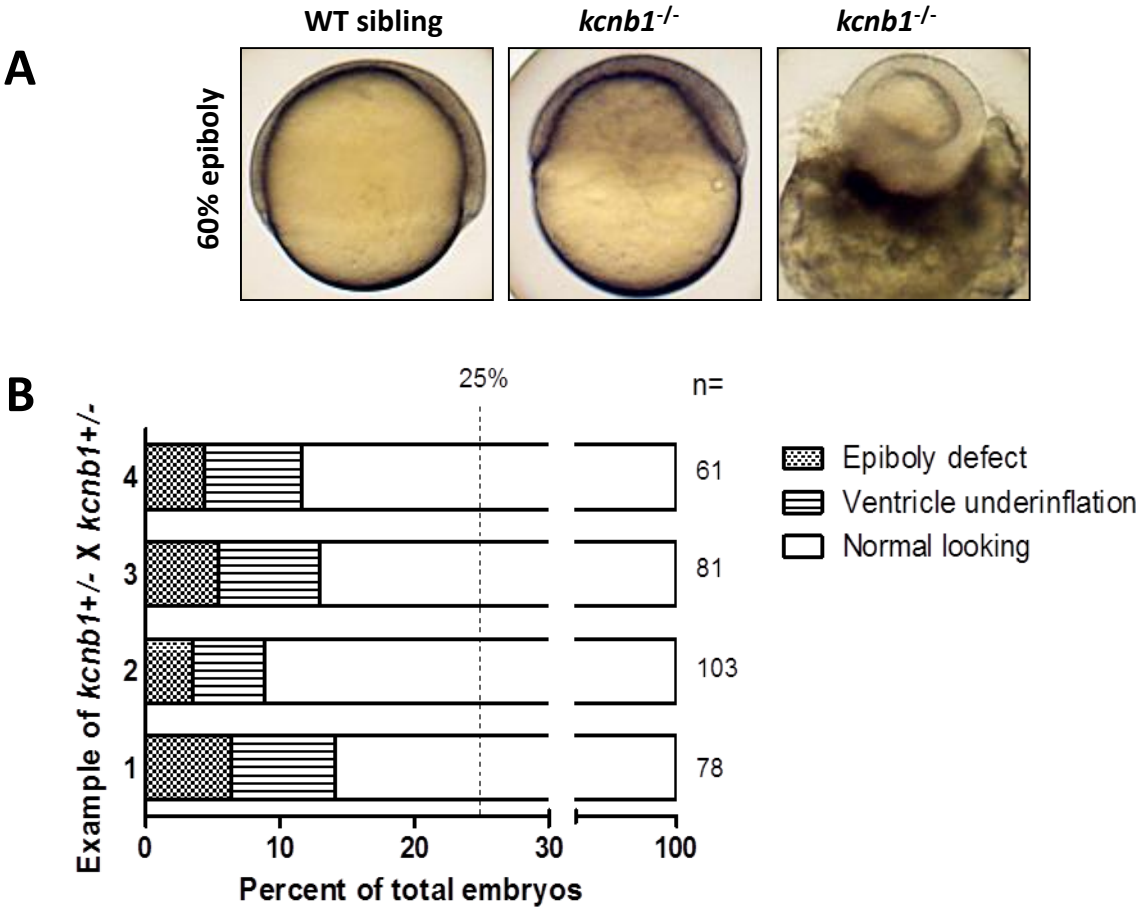

Fig. S8. *kcnb1* mutant embryos also displayed epiboly phenotype at early developmental stages. (A) The epiboly phenotype in the *kcnb1* mutants. (B) The summary of phenotype scoring in *kcnb1*$^{-/-}$ mutants.

Development • Supplementary information